IFNG-producing self-reactive CD4$^+$ T cells drive autoimmune adrenalitis in a mouse model of Addison's disease

Arina Andreyeva[1], Juraj Michalik[1], Veronika Niederlova[1], Veronika Cimermanova[1,2], Ales Drobek[1], Radislav Sedlacek[3], Jan Prochazka[3], Juraj Labaj[3], Olha Fedosieieva[3], Waldemar Kanczkowski[4], Peter Draber[5], Ondrej Stepanek[#,1], Ales Neuwirth[#,1]

1 Laboratory of Adaptive Immunity, Institute of Molecular Genetics of the Czech Academy of Sciences, Prague, Czechia

2 Faculty of Science, Charles University, Prague, Czechia

3 Czech Centre for Phenogenomics & Laboratory of Transgenic Models of Diseases, Institute of Molecular Genetics of the Czech Academy of Sciences, Vestec, Czechia

4 Department of Internal Medicine III, University Hospital Carl Gustav Carus, Technische Universität Dresden, Dresden, Germany

5 Department of Immunobiology, University of Lausanne, Epalinges, Switzerland

Correspondence should be addressed to Ondrej Stepanek, ondrej.stepanek@img.cas.cz and Ales Neuwirth, ales.neuwirth@img.cas.cz

Abstract

Autoimmune Addison's disease (AD) is a rare, life-threatening endocrine disorder caused by immune-mediated destruction of the adrenal cortex. AD frequently occurs in patients with autoimmune polyglandular syndrome type 1, a monogenic autoimmune syndrome caused by AIRE deficiency. The pathogenesis of AD remains poorly understood due to the lack of suitable animal models. Here, we established a mouse model of Experimental Autoimmune Adrenalitis by targeting the adrenal self-antigen CYP11A1. Immunization with CYP11A1-derived peptides elicited clonal expansion of CYP11A1-specific T-cell clones and the adrenal infiltration of CD4$^+$ and CD8$^+$ T cells and myeloid cells. Inflammation progressed to granulomatous lesions and culminated in adrenal insufficiency in AIRE-deficient mice with impaired central tolerance. A modification of the model based an adoptive transfer of polyclonal CYP11A1-stimulated CD4$^+$ T cells into T-cell deficient hosts accelerated adrenal dysfunction. In contrast, IFNG-deficient CD4$^+$ T cells induced only mild granulomatous inflammation and failed to cause overt adrenal insufficiency. These findings established a tractable mouse model for dissecting AD pathogenesis and identified CD4$^+$ T cell-derived IFNG as a key effector of adrenal autoimmunity, providing a preclinical platform for testing targeted immunotherapies.

Key words: Addison's disease, adrenals, autoimmunity, CYP11A1, CD4$^+$ T cells, tolerance, IFNG, mouse model

Introduction

Addison's disease (AD) is a primary adrenal insufficiency caused by autoimmune destruction of hormone-producing adrenocortical cells with a prevalence of 1 in 10,000 (Mitchell and Pearce, 2012). AD leads to insufficient production of adrenocortical steroid hormones, which is fatal if untreated. Current management of AD is a life-long replacement therapy with cortisol and aldosterone by their synthetic analogs hydrocortisone and fludrocortisone, respectively (Husebye et al., 2021). However, treatments do not fully mimic physiological hormone regulation, particularly under stress, leaving patients vulnerable to life-threatening adrenal crises (Dineen et al., 2019). Moreover, hormone replacement therapy leads to adverse effects such as osteoporosis, increased blood pressure, obesity or abnormal glucose metabolism (Johannsson et al., 2015; Kobza et al., 2021).

Historically, AD was frequently associated with tuberculosis, when the mycobacterial spread to the adrenal glands induced direct granulomatous destruction of adrenal tissue (Vinnard and Blumberg, 2017). Currently, approximately 40% of AD cases are isolated autoimmune endocrinopathies, while the remaining cases occur in association with other autoimmune disorders, such as thyroiditis or type 1 diabetes (Betterle et al., 2002; Husebye et al., 2021). Most notably, AD often manifests in patients with Autoimmune Polyendocrine Syndrome Type 1 (APS-1). This rare monogenic disorder is caused by mutations in the *AIRE* gene (Finnish-German, 1997; Nagamine et al., 1997), which leads to the emergence of autoreactive T cells in the periphery. Genetic predispositions to AD also involve polymorphisms in genes related to antigen presentation (HLA alleles DR3/DQ2 and DR4.4/DQ8; CIITA) and regulation of T-cell signaling (CTLA-4, PD-1, PTPN22) (Bratland and Husebye, 2011). Furthermore, emerging cancer immunotherapies, particularly immune checkpoint inhibitors, have been reported to induce AD as an adverse effect (Grouthier et al., 2020; Tan et al., 2019).

The hallmark of AD is the presence of autoantibodies against steroidogenic enzyme, 21-hydroxylase (21-OH, CYP21A2) (Erichsen et al., 2009; Winqvist et al., 1992). These circulating antibodies serve as a predictive marker detectable even during the subclinical phase (Betterle et al., 1983). Additionally, it is noteworthy that autoantibodies targeting cholesterol side-chain cleavage enzyme (CYP11A1) are less prevalent (Brozzetti et al., 2010; Chen et al., 1996) but observed in 70 % of individuals with APS-1 (Brozzetti et al., 2010; Ferre et al., 2016). Previous findings support an autoimmune-based mechanism in which self-reactive T cells play a crucial role in AD progression (Bratland et al., 2009; Rottembourg et al., 2010). Both $CD4^+$ and $CD8^+$ T cells specific to immune-dominant epitopes of 21-OH are detected in the blood of the majority of patients with AD (Dawoodji et al., 2014; Rottembourg et al., 2010). After in vitro antigen re-stimulation using 21-OH, a portion of $CD4^+$ T cells produce IFNG suggesting that AD might be a T helper 1 cell (Th1)-associated autoimmune disorder (Dawoodji et al., 2014). However, the mechanism underlying the destruction of adrenocortical cells remains elusive. The understanding of AD etiology has been hindered by the absence of a defined mouse model, and the unavailability of adrenal samples from AD patients, due to unjustified invasiveness of adrenal biopsies from living donors and the rarity of the disease.

Here, we present a novel mouse model of Experimental Autoimmune Adrenalitis resembling AD. Immunization with immunogenic CYP11A1 peptides induces a robust and heterogeneous $CD4^+$ T cell response, leading to adrenal inflammation, pathological changes, and decreased adrenal production of corticosterone, a murine analog of cortisol. We identified IFNG production by CYP11A1-reactive $CD4^+$ T cells as the key molecular mechanism driving the disease progression and thus, a potential therapeutic target for treating AD. Overall, this model not only provides a platform for investigating the mechanisms underlying adrenal failure but also serves as a valuable tool for preclinical testing of novel therapies.

Results

Immunization with CYP11A1-derived peptides drives the infiltration of effector CD4$^+$ T cells into the adrenal glands

Attempts to generate a mouse model of Addison's disease using 21-OH, the primary human autoantigen, were unsuccessful. To overcome immune tolerance to adrenal antigens, we searched for an alternative candidate expressed both in adrenocortical cells and in the thymus in an AIRE-dependent manner. Our reanalysis of murine thymic single-cell RNA sequencing (scRNA-seq) data (Nishijima et al., 2022) revealed that *Cyp11a1* is expressed in medullary thymic epithelial cells (mTECs) in an AIRE-dependent manner, similar to the canonical tissue-restricted gene *Ins2*, whereas *Cyp21a1* (encoding mouse 21-OH) expression was nearly undetectable in the thymus (Figure 1A, Figure S1A). Based on these criteria, CYP11A1—previously identified as a target of autoantibodies in APS-1 patients (Brozzetti et al., 2010; Ferre et al., 2016)—emerged as a strong candidate antigen for inducing autoimmune adrenalitis.

To design immunogenic peptides, we used the Immune Epitope Database (Vita et al., 2019) and identified two candidates (CYP11A1$_{150\text{-}164}$ and CYP11A1$_{233\text{-}247}$) predicted to have the highest binding affinities for the I-A^b MHC class II molecule, which is expressed in C57BL/6J (B6) mice (Figure S1B). We subcutaneously immunized B6 mice with both peptides (pCYP11A1) emulsified in complete Freund's adjuvant (CFA). Two weeks after the immunization, we observed more pronounced adrenal infiltration of CD4$^+$ T cells in the immunized mice than in CFA-only injected controls with a relatively high variability among individual mice (Figure 1B, Figure S1C). On average, 20% of adrenal infiltrating CD4$^+$ T cells expressed IL17A, 10% of them produced IFNG, and 6% were FOXP3$^+$ regulatory T cells (Tregs) without substantial differences between immunized and CFA-only control mice (Figure 1C, Figure S1D). Thus, our data demonstrated that immunization of B6 mice with pCYP11A1 induces an immune response characterized by the adrenal infiltration of heterogeneous CD4$^+$ T cells.

Adrenal CD4$^+$ T cells clonally expand and display diverse effector fates

To address the diversity of adrenal infiltrating CD4$^+$ T cells in detail, we performed single-cell transcriptomics combined with TCRαβ sequence V(D)J profiling of CD4$^+$ T cells isolated from three mice with high CD4$^+$ T-cell adrenal infiltration determined by flow cytometry at two weeks after immunization (Figure S2A). As a control, adrenal CD4$^+$ T cells from six CFA-immunized mice were pooled to obtain sufficient cell numbers (Figure S2A). Splenic CD4$^+$ T cells from both groups of mice were analyzed as well.

Unsupervised clustering identified thirteen distinct clusters of adrenal and splenic CD4$^+$ T cells (Figure S2B). Upon our manual annotation of these clusters, five of them represented naïve T cells and were merged into a single cluster in the final projection (Figure 1D). In the control adrenals, CD4$^+$ T cells were predominantly composed of iNKT cells with a limited presence of effector cells (Figure 1F). In contrast to the spleen with predominating naïve CD4$^+$ T cells, the majority of adrenal CD4$^+$ T cells displayed an effector phenotype (*Cd44*$^+$, *Icos*$^+$, *Sell*$^-$, *Ccr7*$^-$) (Figures 1E-F, Figure S2C). Among the *Cd44*$^+$ antigen-experienced T cells (Figure S2C), eight clusters were annotated based on specific gene markers and/or V(D)J usage: Th1 cells (*Ifng*$^+$, *Tbet*$^+$), Th1-like cells (*Ifng*$^+$, *Tbet*$^+$, *Ccl5*$^+$), Th17 cells (*Il17a*$^+$, *Rorc*$^+$, *Ccr6*$^+$), activated Tregs (aTregs) (*Foxp3*$^+$, *Ikzf2*$^+$, *Tigit*$^+$), naïve Tregs (*Foxp3*$^+$, *Ikzf2*$^+$), Tfh (*Bcl6*$^+$, *Nr4a1*$^+$, *Lag3*$^+$, *Pdcd1*$^+$), CD4$^+$ iNKT cells (*Nkg7*$^+$, *Cd160*$^+$, CDR3α: CVVGDRGSALGRLHF) and memory T cells (*Ccr7*$^+$, *Tcf7*$^+$) (Figure 1G, Figures S2D-E).

To our knowledge, the Th1-like IFNG-expressing cells, which differed from canonical Th1 cells by the expression of *Ccl5*, *P2rx7, Il2*, *Zfp683* (*Hobit*), *Bcl2* and a lack of NK-related genes *Ifitm1*, *Klrc1*, and *Klrd1*, have not been previously described (Figures 1G-H, Figure S2D).

The naïve Treg cluster detected in the spleen was almost absent in the adrenals (Figures 1E-F). Instead, adrenal Tregs exhibited an activated phenotype, as demonstrated by substantial changes in gene expression, including increased expression of *Tigit*, *Lag3*, *Hif1a*, *Klrg1*, *Pdcd1*, *Id2, Ccr2*, *Ccr4*, *Foxp3*, and lower expression of *Bcl2* and *Il2ra* (Figures 1G, I).

Th17 and memory $CD4^+$ T cells were enriched in all three immunized mice in comparison to the control sample, which comprised pooled adrenal $CD4^+$ T cells from CFA-only treated mice (Figure 1J, Figure S2F). Inversely, the frequencies of naïve $CD4^+$ cells and iNKT cells were higher in the control samples than in the immunized mice. Two mice showed strongly enriched Th1 cells, whereas the third one had elevated Th1-like and aTreg cells illustrating the mouse-to-mouse variability (Figure 1J).

To complement these phenotypic observations with gene-level analysis, we performed gene set enrichment analysis (GSEA) on adrenal $CD4^+$ T cells from peptide-immunized versus control mice. This revealed enrichment of TNF, IL-2, and IFNG–associated gene signatures upon pCYP11A1 immunization (Figure 1K). Additionally, differential expression analysis across all experimental groups showed upregulation of proinflammatory Th1- and Th17-related genes as well as genes associated with T-cell activation (Figure 1L). These transcriptional changes are consistent with the increased abundance of Th1 and Th17 effector subsets identified by scRNA-seq.

In the next step, we identified clonally expanded families based on their shared TCRα and TCRβ sequences (Figure 2A). The clonally expanded T cells were present primarily within effector populations in the adrenal samples from all three pCYP11A1-immunized mice and only marginally in the spleen (Figure 2B, Figure S2G). Th17, Th1-like, Tfh, Th1, aTreg and memory cells were the subsets with substantial clonal expansion (Figure 2C).

Most clones exhibited a bias toward a specific lineage phenotype, with a predominance of the Th17 lineage, followed by aTreg, Tfh, and Th1-like subsets. Approximately one-third of the clones displayed a multidirectional effector phenotype. Notably, many of the clones with a dominant Th17 bias also gave rise to Th1 cells (Figure 2D). To investigate antigen specificity, we selected four representative clones with distinct effector profiles (Figure 2E) and generated retrogenic mice expressing individual TCRs. Two clones, designated ADR1 (original Th1/Th17 cells) and ADR3 (original Tfh cells), successfully produced monoclonal $CD4^+$ T-cell populations in vivo. In subsequent in vitro antigen recall assays, both ADR1 and ADR3 expressing T cells specifically responded to antigen-presenting cells loaded with $CYP11A1_{233\text{-}247}$ peptide, but not to $CYP11A1_{150\text{-}164}$ or unloaded controls (Figure 2F). These results demonstrate that pCYP11A1 immunization drives adrenal infiltration by $CD4^+$ T cells with canonical helper phenotypes as well as unique Th1-like cells, and that at least a subset of these clones are reactive to the adrenal self-antigens.

The development of the Experimental Autoimmune Adrenalitis model

Because the single-dose immunization induced a robust $CD4^+$ T-cell infiltration only in some experimental animals, we modified the protocol to administer a booster injection with the peptides combined with poly(I:C) as adjuvant and costimulatory anti-CD40 antibodies at two weeks post-immunization (Kumai et al., 2017). Flow cytometry analysis performed a week after the booster revealed that the second antigen dose enhanced the adrenal infiltration of $CD4^+$ T cells together with $CD8^+$ T cells, B cells and $CD11b^+$ myeloid cells (Figure 3A, Figure S3A). For this reason, we used this

two-step immunization scheme in the subsequent experiments. Henceforth, we refer to this protocol as Experimental Autoimmune Adrenalitis (EAA).

We characterized the $CD4^+$ T cells in EAA using flow cytometry panels inspired by the scRNA-seq data (Figures 1D, G, Figure S2D) to define individual populations of $CD4^+$ T cells ($CD4^+$, $TCR\beta^+$, $CD8\alpha^-$, $NK1.1^-$): Th1 cells ($IFNG^+$, $CCL5^-$), Th1-like cells ($IFNG^+$, $CCL5^+$), Th17 cells ($IL17A^+$), and Tregs ($FOXP3^+$) upon PMA/ionomycin restimulation (Figure S3B). To exclude contamination with blood leukocytes, we administered a fluorescently labeled anti-CD45-PE antibody intravenously 15 minutes before euthanasia. Additionally, we used two different experimental control groups – non-treated mice (NT) and mice that underwent the two-step mock immunizations without the peptides (Ctr). We observed that the EAA mice had higher numbers of $CD4^+$ T cells (Figure 3B) and all studied effector subsets (i.e., Th1, Th1-like, Th17, and Tregs) (Figure 3C, Figure S3C).

We observed significant infiltration of IFNG-expressing $CD8^+$ T cells, but not NK cells, in the EAA mice compared to the controls (Figure 3D). Notably, the mock immunization induced detectable infiltration of $IFNG^+$ $CD8^+$ T cells as well, but to a lesser extent than the EAA protocol (Figure 3D).

To assess the spatial localization of immune infiltrates, we performed histological analysis of adrenal glands. Leukocytes were primarily localized within the zona fasciculata (the site of corticosterone production) of the adrenal cortex, with some extension toward the juxtamedullary boundary and medulla (Figure 3E). This was confirmed by the detection of $CD45^+$ and $CD4^+$ T cells by immunofluorescence (Figure 3F). These results demonstrate that the immune cell infiltration in the EAA mice largely corresponds to the pattern observed in AD patients (Kemp et al., 2016; Krywanczyk and Bundock, 2017).

Overall, our data demonstrated that the EAA protocol elicits a strong immune response, characterized by the specific recruitment of inflammatory cells preferentially to the adrenal cortex, the site of extensive steroidogenesis.

CYP11A1 administration induces pathological and functional changes in adrenocortical cells

We investigated whether immune cell infiltration of the adrenal gland affects its morphology and endocrine function. Hematoxylin and eosin staining of adrenal tissue sections executed three to five months after EAA induction revealed the presence of enlarged, multinucleated foamy cells (Figure 4A) with a high lipid content (Figure 4B), which exhibited robust autofluorescence in the green spectrum under fluorescence microscopy (Figure 4C). Notably, co-staining with CYP11A1 demonstrated that these lipogenic structures within the adrenal cortex were CYP11A1-negative (Figure 4C). Immunohistochemical analysis further showed that these structures were F4/80-positive, indicating a cortical macrophage component (Figure 4D). Based on these features, we consider these structures to be granulomas, a histopathological hallmark of the adrenals in tuberculosis-driven Addison's disease (Tran et al., 2021). Quantification of the granulomas revealed that these structures accounted for approximately 2% of the adrenal cortex at three months post-immunization, increasing to 5% at five months in males (Figure 4E). However, we did not observe EAA-induced granuloma formation in females (Figures S4A-B).

In the next step, we examined the adrenal function in the EAA mice. We measured blood corticosterone levels following ACTH stimulation test, which is the diagnostic test for adrenal sufficiency routinely used in human patients (Bornstein et al., 2016). EAA male mice exhibited a significant reduction in corticosterone production compared to peptide-free immunized control mice (Figure 4F). As with the granuloma formation, we did not observe this effect in females (Figure S4C). For this reason, we used males in the subsequent EAA experiments. Normal blood sodium and

potassium levels, along with an intact zona glomerulosa, indicated preserved mineralocorticoid production (Figure S4D). Overall, these findings demonstrate that the EAA protocol induces progressive adrenal pathology and dysfunction, which largely recapitulates key pathological features of Addison's disease.

AIRE deficiency exacerbates adrenal pathology in the EAA model

Since AIRE-dependent self-antigen expression in the thymus contributes to T-cell tolerance, and CYP11A1 is absent in AIRE-deficient mTECs (Nishijima et al., 2022), we investigated whether *Aire*$^{-/-}$ mice would exhibit increased susceptibility to adrenal pathology in our model. Indeed, both hallmarks of EAA - granuloma formation and reduced corticosterone production - were significantly enhanced in the *Aire*$^{-/-}$ mice (Figures 4G-H). Notably, five months post-immunization, *Aire*$^{-/-}$ mice exhibited a markedly increased degree of granuloma formation compared to wild-type B6 mice (Figure 4E). Next, we tested whether tumor necrosis factor (TNF), a pro-inflammatory cytokine contributing to several autoimmune and inflammatory disorders (Bradley, 2008), is involved in the EAA induction. Although TNF signaling appeared relevant in our transcriptional analyses, *Tnfr1*$^{-/-}$ mice lacking the major TNF receptor displayed similar levels of granuloma formation as controls, suggesting that the TNF signaling is not essential for EAA induction (Figure 4I). These findings underscore the critical role of AIRE-mediated central tolerance in protecting against adrenal autoimmunity, highlighting that the absence of thymic expression of CYP11A1 increases susceptibility to autoimmune adrenal inflammation.

An adoptive transfer EAA model of CYP11A1-restimulated CD4$^+$ T cells accelerates adrenal pathology

To investigate the direct role of CD4$^+$ T cells in disease progression, we modified the EAA protocol (Figure 5A). B6 mice were first immunized with pCYP11A1 in CFA, while control mice received CFA alone. Ten to eleven days post-immunization, lymph node cells were harvested and cultured for three days in the presence of pCYP11A1. CD44$^+$ CD4$^+$ T cells were then sorted and adoptively transferred into T cell-deficient (*Cd3e*$^{-/-}$) or B cell and T cell-deficient (*Rag2*$^{-/-}$) recipient mice, followed by the standard EAA immunization protocol, including booster injection. In both recipient strains, the adoptive transfer of CYP11A1-restimulated CD4$^+$ T cells accelerated disease onset and increased its penetrance, as evidenced by impaired corticosterone production and extensive granuloma formation three months post-EAA induction (Figures 5B-C). Additionally, the histological and flow cytometry examination revealed a high degree of leukocyte infiltration (mainly CD4$^+$ T cells) in the cortical zona fasciculata (Figure 5D-E). These findings demonstrate that CD4$^+$ T cells alone are sufficient to induce EAA, while CD8$^+$ T cells and B cells are dispensable. Altogether, this adoptive transfer model, which induces a faster and more robust disease response, presents a valuable alternative platform for preclinical testing of therapeutic interventions.

IFNG is a therapeutic target in Addison's disease

CD4$^+$ T cells constituted the majority of adrenal-infiltrating CD45$^+$ cells in the adoptive transfer EAA model (Figure 5E). Since IFNG-producing CD4$^+$ T cells were present during the early phases of EAA (Figure 3C), we directly assessed the role of CD4$^+$ T cell-derived IFNG by adoptively transferring CYP11A1-restimulated *Ifng*$^{-/-}$ CD4$^+$ T cells. Unlike IFNG-sufficient CD4$^+$ T cells, *Ifng*$^{-/-}$ T cells failed to induce adrenal dysfunction: the recipient mice maintained normal responses to ACTH stimulation (Figure 5F) and exhibited markedly reduced adrenal granuloma formation (Figure 5G). Flow cytometry analysis of adrenal CD4$^+$ T cells revealed greater cellularity and a dominant Th1 polarization in IFNG-sufficient transfers (Figures 5H-I). These findings establish IFNG as a key driver

of adrenal failure and highlight our EAA model as a valuable preclinical platform for identifying therapeutic targets and advancing translational research in autoimmune Addison's disease.

Discussion

In this study, we established a pioneering mouse model of AD that recapitulates a key hallmark of the human disorder – primary adrenal insufficiency. Despite exhibiting milder pathology with the absence of fibrosis, and no adrenal atrophy, our EAA model represents the first murine system to demonstrate progressive autoimmune destruction of the adrenal cortex, the defining characteristic of AD.

Our findings identify $CD4^+$ T cell-derived IFNG as a central molecular driver of EAA pathogenesis. This aligns with clinical data from AD patients, where 21-OH-reactive $CD4^+$ T cells have been shown to produce IFNG (Bratland et al., 2009; Dawoodji et al., 2014). IFNG-driven T-cell responses are also characteristic of patients with APS-1 (Oikonomou et al., 2024). Therapeutically, treatment of five APS-1 patients with ruxolitinib, an inhibitor of JAK1/2 kinases that are required for IFNG signaling, has been shown to reduce T cell-derived IFNG levels and improve multiple clinical manifestations, including alopecia, oral candidiasis, nail dystrophy, gastritis, enteritis, arthritis, Sjögren's-like syndrome, urticaria, and thyroiditis (Oikonomou et al., 2024). Given that AD is a common manifestation of APS-1 (Ahonen et al., 1990; Husebye et al., 2009), these findings raise the possibility that inhibition of IFNG signaling may also modulate adrenal-reactive $CD4^+$ T cells and potentially preserve adrenal steroidogenic function. Because the transition from subclinical adrenalitis to overt adrenal insufficiency is often slow and may be predicted by the presence of 21-OH autoantibodies (Coco et al., 2006; Laureti et al., 1998), targeted immunotherapy aimed at suppressing IFNG signaling may provide a window of opportunity to intervene early and prevent irreversible adrenal damage.

Previous therapeutic efforts to restore endogenous glucocorticoid production in newly diagnosed AD patients, which combined B-cell depletion (rituximab) with ACTH-mediated adrenal stimulation, failed to reverse adrenal insufficiency (Napier et al., 2020). Our data in *Rag2*$^{-/-}$ mice, which lack B cells and still develop robust disease, demonstrate that B cells are dispensable for EAA pathogenesis. These findings suggest that therapeutic strategies suppressing the effector functions of autoreactive $CD4^+$ T cells, rather than B cells, have the potential to preserve the adrenal function in AD.

IFNG-dependent granuloma formation in the EAA model, as well as granulomatous adrenal inflammation in tuberculosis-driven AD (Tran et al., 2021), underscores a critical role for Th1-mediated macrophage polarization in adrenal pathology. The functional significance of these granulomas, which accumulate progressively and can occupy up to 20% of the adrenal cortex during EAA, remains unclear. The pro-inflammatory environment likely compromises adrenocortical cell viability (Kanczkowski et al., 2013), disrupts metabolic homeostasis (Mateska et al., 2023), and impairs steroidogenic function. We hypothesize that excessive inflammation in EAA leads to adrenocortical cell destruction and the accumulation of partially degraded, lipid-rich cellular debris that is inefficiently cleared by tissue-resident or recruited macrophages. This impaired clearance may promote the formation of foamy macrophage aggregates within the adrenal cortex. Supporting this notion, lipid-laden foamy macrophages have been reported to accumulate in the adrenal cortex of mice in an age- and diet-dependent manner (O'Brien et al., 2023). Intriguingly, structurally similar syncytial lipoid aggregates have been observed in 18-week-old male mice harboring a *Cyp11a1* promoter mutation that causes adrenal-specific steroidogenic deficiency (Shih et al., 2008), suggesting that impaired steroidogenesis and chronic inflammation may converge on common tissue remodeling pathways. Notably, sex-related differences in macrophage composition (Dolfi et al., 2022) and the higher adrenocortical cell turnover observed in females (Grabek et al., 2019) may contribute to their relative resistance to granuloma formation. However, due to the limited availability of autopsy material from AD patients, it remains challenging to determine whether

granuloma formation is a general feature of human AD or specific to particular etiologies such as APS-1.

To date, a robust and widely accepted murine model of AD has been lacking. Previous attempts, such as repeated immunization with adrenal extracts and lipopolysaccharide, elicited only mild cortical inflammation without inducing overt adrenal insufficiency, even after prolonged exposure (Fujii et al., 1992). These data underscore the notion that immune cell infiltration alone is insufficient to trigger endocrine failure, a concept supported by autopsy findings showing focal adrenal lymphocytic infiltration in up to 7% of individuals under 54 years of age (Hayashi et al., 1989), a frequency that far exceeds the clinical incidence of AD. This discrepancy suggests that many immune responses targeting the adrenal cortex may remain subclinical or abortive. Mitchell and Pearce (2012) proposed that high intra-adrenal glucocorticoid concentrations establish a locally immunosuppressive microenvironment, limiting immune effector function. This, in conjunction with the presence of intraglandular regulatory T cells, may explain the delayed onset of adrenal dysfunction in our model, despite the accumulation of autoreactive $CD4^+$ T cells.

Our data highlight CYP11A1 as a physiologically relevant adrenal autoantigen capable of eliciting a robust $CD4^+$ T cell-mediated autoimmune response. While clinical diagnosis relies on 21-OH autoantibodies, the prevalence of AD in APS-1 and the AIRE-dependent expression of *Cyp11a1* in mTECs (Hubert et al., 2009) argue for its central role in tolerance and adrenal autoimmunity. Single-cell RNA-sequencing revealed that *Cyp11a1* is expressed in a subset of $AIRE^+$ mTECs in a mosaic pattern, consistent with promiscuous gene expression observed in the thymus (Brennecke et al., 2015; Derbinski et al., 2008), whereas *Cyp21a1* expression was more restricted. Although steroidogenic properties have been proposed for TECs (Taves et al., 2023), the enhanced susceptibility of *Aire*$^{-/-}$ mice to EAA supports a critical role for central tolerance to CYP11A1. Future studies employing peptide-MHC class II tetramers will be essential to determine whether thymic deletion or peripheral regulation governs the fate of CYP11A1-specific $CD4^+$ T cells. Both tested adrenal infiltrating T-cell clones recognized the $CYP11A1_{233-247}$ self-peptide, which validated the bona fide autoimmune nature of EAA.

Our findings, together with evidence of progressive adrenal destruction and the intrinsic regenerative capacity of the adrenal cortex (Bornstein et al., 2020; Freedman et al., 2013; Grabek et al., 2019), position the adoptive EAA model as a robust platform for studying the etiology of AD and for preclinical testing of therapeutic interventions targeting autoimmune adrenalitis.

Methods

Mice

Male and female mice aged 6 to 13 weeks at the start of the experiments were used in this study. Whenever possible, age- and sex-matched animals were used; littermates were used when available and evenly distributed among experimental groups. Group allocation was based on animal ID without prior contact with the experimenter to minimize bias. All the mice had a C57BL/6J (B6) genetic background (Charles River). *Cd3e*$^{-/-}$ (RRID:IMSR_JAX:004177, #004177) (Sommers et al., 2000), Ly5.1 (RRID: IMSR_JAX:002014, #002014) (Shen et al., 1985), *Aire*$^{-/-}$ (RRID:IMSR_JAX:004743, #004743) (Anderson et al., 2002), *Rag2*$^{-/-}$ (RRID:IMSR_JAX:008449, #008449) (Hao and Rajewsky, 2001), *Tnfr1*$^{-/-}$ (Ujevic et al., 2024) and *Ifng*$^{-/-}$ (Borst et al., 2020) strains were described. Mice were bred and maintained in a specific pathogen-free facility at the Institute of Molecular Genetics of the Czech Academy of Sciences (IMG) in compliance with Czech Republic regulations. All animal procedures were approved by the Czech Academy of Sciences (AVCR 6917/2022 SOV II) and conducted in accordance with the ARRIVE Essential 10 guidelines (https://arriveguidelines.org/). Mice were housed under a 12-h light/dark cycle at 22±1°C and 55±5% relative humidity, with ad libitum access to reverse osmosis-filtered water and an irradiated standard rodent diet.

Antibodies

Fluorescently labeled antibodies were purchased from BioLegend: CD4-BV650 (clone RM4-5), CD4-AF594 (clone GK1.5), CD4-AF647 (clone RM4-5), CD4-PE (clone H129.19); CD8a-BV510 (clone 53-6.7), CD8a-BV650 (clone 53-6.7); CD11b-BV421 (clone M1/70); CD19-FITC (clone 1D3/CD19); CD25-BV605 (clone PC61); CD44-FITC (clone IM7); CD45-AF700 (clone 30-F11), CD45-AF594 (clone 30-F11); CD45.2-PE (clone 104), CD45.2-AF488 (clone 104); CD62L-APC (clone MEL-14); CD69-PerCP-Cy5.5 (clone H1.2F3); TCRβ-PE (clone H57-597), TCRβ-Pacific Blue (clone H57-597); NK-1.1-BV785 (clone PK136); IFNG-AF700 (clone XMG1.2); FOXP3-AF488 (clone 150D); CCL5-Pe-Cy7 (clone 2E9/CCL5). IL17A-APC (clone eBio17B7) and Goat anti-rabbit-AF647 were purchased from Invitrogen. Biotinylated anti-CD4 antibody was purchased from Biolegend (clone RM4-5). Fc blocking CD16/CD32 antibody (clone 2.4G2) was purchased from BD Bioscience. CYP11A1 (clone D8F4F, rabbit) and F4/80 (clone D2S9R, rabbit) were purchased from Cell Signaling Technology. ZytoChem Plus (HRP) Polymer anti-Rabbit secondary antibody was purchased from Zytomed systems. InVivoPlus anti-mouse CD40 antibody (clone FGK4.5/FGK45) was purchased from Bio X Cell.

Immunogenic Peptides

I-A^{b} MHCII-restricted immunogenic peptides of CYP11A1 (cytochrome P450 family 11 subfamily A member 1, NCBI Reference Sequence: NP_031830.2) were designed using the Immune Epitope Database (IEDB.org). Two peptides with the highest predicted binding affinities and non-overlapping positions within the CYP11A1 protein were selected: CYP11A1$_{233-247}$, AVYQMFHTSVPMLNL, and CYP11A1$_{150-164}$, VLNQEVMAPGAIKNF. Peptides were synthesized at crude purity (70–85%) by Peptides & Elephant. To prevent degradation, peptides were dissolved in dimethyl sulfoxide (DMSO, Sigma-Aldrich), aliquoted, and stored at −80°C at a concentration of 20 mM.

Experimental Autoimmune Adrenalitis (EAA) Model

Mice aged 8 to 13 weeks were subcutaneously immunized with 100 µg of each peptide emulsified in Complete Freund's Adjuvant (CFA), which consisted of Incomplete Freund's Adjuvant (Sigma-Aldrich) supplemented with 4 mg/ml of heat-inactivated *Mycobacterium tuberculosis* H37RA (BD Difco). Immunizations were administered at two dorsal injection sites per mouse. A booster injection was

delivered intraperitoneally (i.p.) 10–14 days later, containing 100 µg of each peptide, 50 µg of high molecular weight poly(I:C) (InvivoGen), and 100 µg of anti-CD40 antibody (clone FGK4.5/FGK45).

Adoptive Transfer Model

B6 or *Ifng*$^{-/-}$ mice were immunized subcutaneously with 100 µg of each CYP11A1 peptide (pCYP11A1) emulsified in CFA. Ten days post-immunization, lymphocytes were isolated from the axillary, inguinal, cervical, and mesenteric lymph nodes and cultured in complete RPMI medium (Sigma-Aldrich) (10% FBS (Gibco), 100 U/ml penicillin (BB Pharma), 100 µg/ml streptomycin (CELLPURE)) for 3 days in the presence of pCYP11A1 (10 µg/ml). At 24 h, recombinant interleukin-2 (Gibco) was added to the culture at a concentration of 2 ng/ml. On day 3, CD4$^+$ T cells were enriched by magnetic separation using biotinylated anti-CD4 antibody (clone RM4-5) and anti-biotin magnetic beads (Miltenyi Biotec; LS columns or AutoMACS separator). After staining with CD44-FITC (clone IM7), CD62L-APC (clone MEL-14), and CD4-PE (clone H129.19), activated CD4$^+$CD44$^+$ T cells were subsequently sorted by flow cytometry, and 1×10^5 cells were transferred intravenously (i.v.) into *Rag2*$^{-/-}$ or *Cd3e*$^{-/-}$ recipient mice. The following day, recipient mice underwent the EAA induction protocol, including both primary and booster immunizations as described above. For the control group, an equivalent number of CD4$^+$CD44$^+$ T cells were isolated and transferred from CFA-only–immunized donor mice without in vitro expansion. To ensure synchronized cell harvest and transfer, CFA-only control donors were immunized three days later than the peptide-immunized mice.

Flow Cytometry and Cell Sorting

Adrenal glands were digested in 1.5 ml microtubes containing Collagenase D (0.5 mg/ml) and DNase I (0.1 mg/ml) (both from Roche) in complete RPMI medium. Glands were incubated at 37°C for 5 min, minced with scissors, and incubated for an additional 20 min with continuous shaking. During digestion, tissues were gently disrupted at least once by reverse pipetting using wide-bore 1.5 ml tips. Following digestion, samples were transferred to 24-well tissue culture plates, and remaining tissue fragments were passed through a 70 µm nylon mesh using syringe plungers. Cells were washed with 1× HBSS supplemented with 2% FBS and 200 mM EDTA. Surface staining was performed in this buffer for 30 min on ice using fluorochrome-conjugated primary antibodies and LIVE/DEAD Fixable Near-IR viability dye (Thermo Fisher Scientific) in the presence of Fc blocking CD16/CD32 antibody (clone 2.4G2).

For intracellular staining, cells were fixed and permeabilized with the Foxp3/Transcription Factor Staining Buffer Set (Invitrogen) according to the manufacturer's instructions. For cytokine detection, cells were stimulated with phorbol 12-myristate 13-acetate (PMA; 50 ng/ml; Sigma-Aldrich) and ionomycin calcium salt (1 µM; Sigma-Aldrich) at 37°C for 3–4 h in the presence of protein transport inhibitor cocktail (Golgi Block, Invitrogen). In some experiments, to exclude blood leukocytes, CD45.2 PE (clone 104) was administered i.p. at 3 µl/mouse in 200 µl PBS for 15 min prior to euthanasia. Fluorescently conjugated antibodies were used at a standard dilution of 1:200 unless otherwise specified. Samples were analyzed on a Cytek Aurora spectral cytometer, and cell sorting was performed on a FACSAriaII (BD Biosciences) or MoFlo Influx (BD Biosciences) sorter. Data were analyzed using FlowJo v10.8.0 (Tree Star).

Adrenal Histology, Immunochemistry and Immunofluorescence

Adrenal glands were removed and carefully cleaned of surrounding fat under a stereomicroscope, then fixed in 4% formaldehyde (Sigma-Aldrich) in PBS for 3h. After fixation, samples intended for paraffin embedding were transferred to 70% ethanol, whereas samples for cryosectioning were incubated overnight in 30% sucrose (Sigma-Aldrich) in PBS, embedded in OCT compound (Sakura),

snap-frozen on dry ice, and stored at −80°C. Cryosections (10 µm) were prepared using a Leica CM1950 cryostat (Leica Biosystems, Germany).

Standard hematoxylin and eosin (H&E) staining of paraffin sections was performed at the Czech Centre of Phenogenomics according to internal standard operating procedures. Tissue processing was performed using a Leica ASP6025 automated vacuum processor, embedding with a Leica EG1150 tissue embedding station, and sectioning at 4 µm using a Leica RM2255 rotary microtome. Representative sections were stained with hematoxylin (Sigma-Aldrich) and eosin (Carl ROTH) using a Leica ST5020 automated stainer, then coverslipped using a Leica CV5030 coverslipper (all Leica Biosystems, Germany). Images were acquired on an Axio Scan.Z1 slide scanner (Zeiss, Germany).

In some experiments, H&E staining was performed on cryosections. Cryosections were fixed in acetone (Carl ROTH) for 15 min and air-dried for 20 min. Sections were stained with hematoxylin M (Biognost) for 1–2 min, rinsed in water, differentiated in 0.1% hydrochloric acid (Penta Chemicals) for 10 s, rinsed again, and stained with eosin Y (Biognost) for 1 min. Slides were dehydrated in 96% ethanol for 10–15 min, followed by 1:1 isopropanol/ethanol for 5 min, and cleared in xylene (Lachner) for 2×5 min. Samples were mounted in water-free Solakryl medium, and images were acquired at 40× magnification using a Leica DM6000 widefield microscope (Objective: HCX PL APO 40×/0.75 DRY PH2) equipped with a Leica DFC490 camera.

For immunofluorescence staining of infiltrating leukocytes, cryosections were fixed with 4% formaldehyde for 10min, washed in PBS (3×5 min), and blocked in 2.5% FBS in PBS/0.3% Triton X-100 for 1 h at room temperature (RT). Sections were incubated overnight at 4°C with a primary antibodies mix (CD45.2 AF488, CD4 AF647) diluted in PBS/0.3% Triton X-100. The next day, sections were washed in PBS (3×5 min), nuclei were counterstained with DAPI for 15min. For CYP11A1 detection, cryosections were similarly fixed, washed, and blocked in 5% goat serum in PBS/0.3% Triton X-100 for 1 h at RT. Sections were incubated overnight at 4°C with rabbit monoclonal anti-CYP11A1 antibody (diluted 1:100 in PBS/0.3% Triton X-100). The following day, slides were washed with PBS (3×5 min) and incubated with goat anti-rabbit AF647 secondary antibody (diluted 1:1000, 1 h at RT). After final washes with PBS (3×5 min), DAPI staining was performed as described above.

Granulomas were visualized by 488nm laser excitation with emission detection between 495–600nm. Slides were mounted in ProLong Gold Antifade Mountant (Invitrogen) and imaged using a Leica TCS SP8 confocal microscope (Objective: HC PL APO 40×/1.30 OIL CS2).

Immunohistochemistry and Oil Red O staining were performed at the Czech Centre of Phenogenomics according to internal standard operating procedures. For immunohistochemistry for F4/80, formalin-fixed, paraffin-embedded adrenal sections were deparaffinized on a Leica ST5020 system. Antigen retrieval was performed in citrate buffer (pH 6.0) at 110°C for 15 min. Endogenous peroxidase activity was blocked with 3% hydrogen peroxide for 20 min at RT in the dark. Non-specific binding was blocked with 2% BSA for 30 min at RT. Sections were incubated overnight at 4°C with anti-F4/80 (clone D2S9R) XP® rabbit mAb at the dilution 1:750. The HRP-conjugated anti-rabbit secondary antibody (Zytomed systems) was applied for 30 min at RT. Between each step (except between BSA blocking and primary antibody incubation), slides were washed in PBS (3×5 min). The signal was developed using the Dako Liquid DAB+ Substrate Chromogen System for 6 min. Slides were counterstained with Harris hematoxylin (Sigma-Aldrich) for 10 s, dehydrated, and coverslipped using the Leica ST5020 + CV5030 automated system.

For Oil Red O staining to detect lipid inclusions, frozen adrenal sections (8–10 µm) were fixed in 4% paraformaldehyde, rinsed in tap water, and immersed in 60% isopropanol, followed by staining in freshly prepared Oil Red O (CI 26125) (Carl ROTH) working solution for 15min. After staining, sections were dipped in 60% isopropanol, nuclei were lightly counterstained with Harris hematoxylin (a few drops for 20 s) and rinsed in tap water. Sections were mounted with Aquatex® aqueous mounting medium (Sigma-Aldrich).

ACTH Stimulation Test, Serum Collection and Corticosterone Measurement

The ACTH peptide (1–24: SYSMEHFRWGKPVGKKRRPVKVYP) was synthesized at 95% purity by Peptides & Elephant and dissolved in distilled water at a concentration of 1 mg/ml. Mice were injected (i.p.) with dexamethasone (Sigma-Aldrich, 0.1 mg/mouse) at 8:00 a.m. to suppress endogenous corticosterone production. Two hours later, ACTH was administered (i.p.) at 1 mg/kg. At 11:00 a.m., one hour after ACTH injection, blood was collected via superficial facial vein puncture using a sterile lancet. Samples were allowed to clot at room temperature for 30 min, then centrifuged at 1,250 × g for 15 min at 4°C. Serum was harvested and stored at −80°C until analyses. For downstream analyses (e.g. flow cytometry, Na^+/K^+ measurement), mice were rested for at least three days after the ACTH stimulation test to allow for recovery. Corticosterone levels were measured using a commercial ELISA kit (Tecan), following the manufacturer's instructions. Optical density was read using an EnVision plate reader (PerkinElmer), and data were analyzed with MyAssays software.

Na^+/K^+ measurement

Serum sodium and potassium concentrations were measured on a AU480 automated biochemical analyzer (Beckman Coulter) at the Czech Centre of Phenogenomics. The analyzer was calibrated for the tested parameters, including checks for lipemia, icterus, and hemolysis. Samples were then processed automatically according to the instrument's programmed protocols for each parameter.

scRNA-seq

B6 mice (10-12 weeks old) were subcutaneously immunized with 100 µg of each pCYP11A1 emulsified in CFA. Control mice received CFA alone without peptides. Fourteen days post-immunization, adrenals were harvested, cleaned, and processed for flow cytometry and cell sorting as described above. Splenocytes were not enzymatically digested. Prior to sorting, 10% of the cells were stained with fluorochrome-conjugated primary antibodies (TCRβ-AF488, CD4-PE), and adrenal $CD4^+$ T-cell infiltration was quantified by flow cytometry. The remaining cells of the samples with the highest adrenal infiltration were labeled with fluorochrome-conjugated antibodies (TCRβ-AF488, CD4-PE, CD11b-BV421) and individual TotalSeq-C Hashtag antibodies for multiplexing (BioLegend; MH1-MH10). $CD4^+$ T cells were sorted as live, $CD11b^-$, $TCR\beta^+$, $CD4^+$ cells using a MoFlo Influx cell sorter. Cell viability prior to loading was assessed using the TC20 Automated Cell Counter (Bio-Rad, #1450102) and exceeded 90%. Cells were loaded onto a 10x Chromium instrument (10x Genomics). Libraries were prepared using the Chromium Single Cell 5' Library & Gel Bead Kit and the Chromium Single Cell 5' Feature Barcode Library Kit (10x Genomics; #PN-1000014, #PN-1000020, #PN-1000080, #PN-1000009, #PN-1000084, #PN-1000071), following the Feature Barcode technology for Cell Surface Protein protocol (#CG000186 Rev D). The resulting cDNA libraries were sequenced on an Illumina NovaSeq 6000 using the S1 Reagent Kit (100 cycles, Illumina, #20012865).

BCL files were demultiplexed using Cell Ranger bcl2fastq v5.0.1, and reads were aligned using Cell Ranger v5.0.1 to the *Mus musculus* reference genome (GRCm38, Ensembl version 102) (Howe et al., 2021). Downstream processing was performed in R v4.2.1 using Seurat v4.3.0 (Hao et al., 2021). Cells

lacking hashtag expression or containing multiple hashtags were removed. Mitochondrial, ribosomal, and T-cell receptor V/J genes were excluded from further analysis.

Adrenal and spleen samples were initially analyzed separately. Each dataset was normalized, and 2,000 highly variable features were identified, followed by dimensionality reduction and clustering (resolutions: 0.8 for adrenal, 0.9 for spleen). Contaminating clusters were removed, and each subset was reprocessed with a clustering resolution of 0.8. The datasets were then integrated using Seurat's canonical correlation analysis (CCA) method with 1,050 anchors, following the exclusion of cells with >6% mitochondrial content or classified as high-feature outliers. Dimensionality reduction and clustering (resolution = 1.0) were performed on the integrated dataset. Clusters containing naïve T cells were merged, and cell identities were manually annotated. The final dataset included 5,584 cells. GSEA pathways were processed using the R package fgsea (v1.20.0) using the hallmark gene sets from the Molecular Signatures Database obtained with the R package msigdbr (v 7.5.1). Heatmap was created with package pheatmap (v 1.0.12).

V(D)J sequences were obtained using Cell Ranger VDJ, aligned to the murine IMGT reference (Lefranc et al., 2015). Additional VDJ sequences were retrieved using MiXCR v3.0.13 (Bolotin et al., 2015). Cells with more than two TCRα chains, more than one productive TCRβ chain, or more than two non-productive TCRβ chains were excluded as doublets. Cells sharing identical TCRα and TCRβ chains were classified as clones.

Monoclonal Retrogenic T cells

The generation of immortalized bone marrow cells was performed as previously described (Drobek et al., 2018; Ruedl et al., 2008). Briefly, *Rag2*$^{-/-}$ mice were treated with 100 mg/kg 5-fluorouracil (Sigma-Aldrich), and bone marrow cells were harvested five days later. Cells were cultured in complete IMDM medium (10% FBS) supplemented with stem cell factor, IL-3, and IL-6. After two days, proliferating cells were transduced with a NUP98–HOXB4 fusion construct delivered via the retroviral vector pMYs. Viral transduction was performed by centrifugation (1,250 × g, 30°C, 90 min) in the presence of 10 µg/ml polybrene (Sigma). Transduced cells were selected with 1 µg/ml puromycin (Gibco) for two days and stored in liquid nitrogen.

To generate monoclonal CD4$^+$ T cells, immortalized bone marrow progenitors were transduced with a GFP-expressing MSCV vector encoding TCR alpha and beta chains. Spin infection (1,250× g, 30°C, 90min) was performed in the presence of diethylaminoethyl (DEAE)-dextran (Sigma-Aldrich). TCR sequences corresponding to the ADR1–ADR4 clones, identified by scRNA-seq were synthesized by Invitrogen and subcloned into the MSCV vector. Two days after transduction, expanded GFP$^+$ cells were FACS-sorted and transplanted (i.v.) into lethally irradiated (6 Gy) congenic Ly5.1 recipient mice using X-RAD 225XL Biological irradiator (Precision X-Ray). At least 8 weeks post-transplantation, recipients were sacrificed and GFP$^+$Ly5.2$^+$CD4$^+$ T cells were sorted for in vitro recall assays.

In vitro recall assay

Monoclonal CD4$^+$ T cells sorted from retrogenic mice were co-cultured in complete RPMI medium with splenocytes from Ly5.1 mice (pre-treated with ACK lysis buffer to remove erythrocytes) as antigen-presenting cells (APCs), at a 3:1 responder-to-APC ratio in 96-well culture plates. Cells were re-stimulated for 24 h with individual pCYP11A1 (10 µM) or left unstimulated (no peptide). After incubation, cells were harvested and analyzed by flow cytometry. The following fluorochrome-conjugated antibodies were used: CD45.1, CD45.2, CD4, CD25, and CD69. Dead cells were excluded using the LIVE/DEAD Fixable Near-IR viability dye (Thermo Fisher Scientific).

Data and code availability

The raw sequencing data have been deposited in the NCBI Gene Expression Omnibus (GEO) under accession number GSE303645. The code used for analysis has been deposited on GitHub (https://github.com/Lab-of-Adaptive-Immunity/Project_Adrenalitis).

Statistical analyses

Data were analyzed by two-tailed nonparametric Mann-Whitney test with GraphPad5 software. Data are presented as mean ± SEM. Each symbol represents an individual mouse.

Acknowledgement

We gratefully acknowledge Ladislav Cupak for technical assistance, Zdenek Cimburek and Matyas Sima (Flow cytometry facility, IMG) for cell sorting, Sarka Kocourkova and Michal Kolar (Laboratory of Genomics and Bioinformatics, IMG) for cDNA library preparations, Jachym Antonin Harwood (IMG) for advice on the manuscript, and Dominik Filipp (IMG) for providing us with *Aire*$^{-/-}$ mice. AA, VC, VN are students of the Faculty of Science Charles University in Prague.

This project was funded by European Union's Horizon 2020 research and innovation programme under grant agreement No. 101125695 (ERC Starting Grant ActSwiftly to OS), Charles University Grant Agency (No.176624 to VC), Swiss National Science Foundation (320030-227564 to PD), core funding provided by the Institute of Molecular Genetics of the Czech Academy of Sciences (RVO 68378050). Additional support was provided by the Czech Centre for Phenogenomics, financed through LM202303 by MEYS CR, and OP RDE CZ.02.1.01/0.0/0.0/16_013/0001789 (Upgrade of the Czech Centre for Phenogenomics: developing towards translation research, supported by MEYS and ESIF).

Author contributions

Arina Andreyeva: Formal analysis; Investigation; Visualization; Methodology; Writing. **Juraj Michalik:** Data curation; Software; Formal analysis; Writing. **Veronika Niederlova:** Investigation; Visualization. **Veronika Cimermanova:** Investigation; Visualization. **Ales Drobek:** Investigation, Methodology. **Radislav Sedlacek:** Resources; Supervision; Methodology**. Jan Prochazka:** Resources; Supervision; Methodology **Juraj Labaj:** Resources; Supervision; Methodology. **Olha Fedosieieva:** Investigation, Methodology. **Waldemar Kanczkowski:** Investigation; Methodology. **Peter Draber:** Resources. **Ondrej Stepanek:** Conceptualization; Visualization; Resources; Supervision; Funding acquisition; Writing. **Ales Neuwirth:** Conceptualization; Supervision; Formal analysis; Investigation; Visualization; Methodology; Writing.

Declaration of Interests

The authors declare no competing interests

Figures Legends

Figure 1. pCYP11A1 immunization recruits heterogeneous CD4⁺ T cells into the adrenals.
(A) Expression of *Aire, Ins2*, and *Cyp11a1* in thymic epithelial cells (TECs) from *Aire*$^{+/+}$ and *Aire*$^{-/-}$ mice. Re-analysis of scRNA-seq data of 8-week-old female mice (Nishijima et al., 2022). Color intensity indicates average expression level; dot size indicates the proportion of expressing cells.
(B) Representative gating of CD4⁺ and CD8α⁺ T cells infiltrating adrenal glands 14 days post-immunization (p.i.) with pCYP11A1 and quantification of CD4⁺ T cells (2 independent experiments; n=15-27 mice per group).
(C) Frequencies of IFNG⁺, IL17A⁺, and FOXP3⁺ CD4⁺ T cells in adrenal glands following in vitro PMA/ionomycin re-stimulation (2 independent experiments, n=14-27 mice per group).
In **(B)** and **(C)** statistical significance was determined using the two-tailed Mann–Whitney test; P values are indicated. Bars show the mean ± SEM; individual mice are shown as symbols.
(D-L) scRNA-seq data of CD4⁺ T cells from adrenal glands and spleens of pCYP11A1 immunized/control mice at day 14 p.i. Three mice with the highest CD4⁺ T cell infiltration were selected (Figure S2A). The control adrenal sample represents pooled adrenals from six CFA-immunized mice.
(D) Uniform manifold approximation and projection (UMAP) showing individual clusters of naïve and effector CD4⁺ T cells.
(E) UMAP projection showing cells colored by tissue of origin (adrenal/spleen).
(F) Heatmap showing the relative abundance of CD4⁺ T-cell clusters expressed as Z-scores normalized by columns.
(G) Dot plot showing expression of key marker genes used to annotate clusters. Dot size indicates the proportion of expressing cells; color intensity indicates average expression level.
(H) Heatmap comparing gene expression profiles of pro-inflammatory Th1, Th1-like, and Th17 cells from adrenal glands of immunized mice expressed as Z-scores normalized by rows.
(I) Heatmap showing the relative gene expression profiles of activated Tregs in the spleen and adrenal glands, and naïve Tregs expressed as Z-scores normalized by rows.
(J) Ratio of each CD4⁺ T cell population in peptide-immunized mice versus control mice. A dashed line at 1 denotes equal frequency. Each symbol represents one immunized mouse.
(K) Gene set enrichment analysis (GSEA) illustrating enrichment of hallmark gene signatures in CD4⁺ T cells from immunized versus control animals. Positive normalized enrichment scores indicate stronger enrichment of the gene set in immunized samples. P-values were calculated using adaptive multi-level split Monte-Carlo scheme implemented in the fgsea package with Benjamini-Hochberg adjustment for multiple comparisons.
(L) Heatmap shows the relative expression of selected genes in immunized and control samples from the spleen and adrenals. For each gene, the average expression per each sample was calculated using the function AverageExpression from the Seurat package. The values plotted are z-score normalized by rows.

Figure 2. Adrenal CD4⁺ T cells are clonally expanded.
(A) UMAP projection of CD4⁺ T cells from adrenal glands and spleens of pCYP11A1-immunized mice, showing expanded T-cell clones (≥2 cells with the same TCRαβ).
(B) Distribution of expanded CD4⁺ T-cell clones between adrenal glands and spleens in pCYP11A1-immunized mice.
(C) Distribution of expanded CD4⁺ T-cell clones across defined T-cell subsets.

In **(A-C)** color represents clone size, defined by the number of cells sharing the same T-cell receptor (TCR).

(D) Contribution of defined $CD4^+$ T-cell populations within the top 20 expanded T-cell clones. The x-axis represents individual clones (with corresponding cell counts per clone) arranged by effector phenotype diversity, from highly polarized (left) to multi-directional (right). Colors indicate the effector phenotype of each T-cell clone. The dominant effector phenotype (≥50%) for each clone is indicated above.

(E) UMAP projection highlighting the spatial localization of four selected expanded $CD4^+$ T cell clones ADR1-ADR4 among effector populations. Clones are color-coded to reflect their identity.

(F) Experimental outline testing the antigen specificity of two $CD4^+$ T-cell clones generated in retrogenic mice. The expression of CD69 and CD25 activation markers was measured by flow cytometry following the stimulation with $CYP11A1_{150-164}$ or $CYP11A1_{233-247}$ in vitro. Peptide-free incubation serves as control. Representative data of 3 independent experiments.

Figure 3. Experimental Autoimmune Adrenalitis (EAA) model.

(A) Quantification of total immune cells in adrenal glands of control and pCYP11A1-immunized mice (± booster) at day 25 p.i. (n=5-6 mice per group). Bars indicate mean ± SEM; immune cell subsets are color-coded.

(B, C) Quantification of $CD4^+$ T cells and effector $CD4^+$ T-cell subsets in adrenal glands at 3–4 weeks p.i.

(D) Quantification of adrenal-infiltrating $CD8^+$ T cells, $IFNG^+$ $CD8^+$ T cells, and NK cells.

In **(B–D)** statistical significance was determined using the two-tailed Mann–Whitney test; P values are indicated. Bars show the mean ± SEM; individual mice are shown as symbols (2 independent experiments; n=9–19 mice per group). Groups: non-treated (NT), control (Ctr), and EAA.

(E) Representative H&E staining of adrenal gland sections at 3 weeks p.i. (n=4–5 mice per group). Images show whole-organ sections (scale bar: 200 µm) and magnified views (scale bar: 100µm). Asterisks indicate infiltrating leukocytes.

(F) Representative immunofluorescence images of adrenal gland sections stained for DAPI (nuclei, blue), CD45 (green), and CD4 (red). Scale bar: 100 µm.

Figure 4. Long-term adrenal pathology in EAA.

(A) Representative H&E staining of adrenal glands 3-5 months p.i. (n=33–47 mice in Ctr and EAA group, n=9 in NT group). Whole-organ sections (scale bar: 200 µm) and magnified views (scale bar: 100µm); adrenal borders, medulla, and enlarged, multinucleated foamy cells highlighted in yellow.

(B) Representative Oil Red O staining of adrenal sections from EAA mice. Scale bar: 100µm (n=6 mice).

(C) Representative immunofluorescence staining of adrenal sections from EAA mice showing DAPI (nuclei, blue) and CYP11A1 (red). Multinucleated foamy cells appear green due to autofluorescence of a lipid content. Scale bar: 100µm (n=6 mice).

(D) Representative F4/80 antibody staining demonstrating macrophage infiltration in adrenal sections from EAA mice; right panel shows control (no primary antibody). Scale bar: 100µm (n=8 mice).

(E) Frequency of cortical granulomas in B6 mice at 3–4 months p.i. (4 independent experiments, n=24–32 mice per group) and 5 months p.i. (3 independent experiments, n=9–15 mice per group).

(F) Serum corticosterone levels following ACTH stimulation test in B6 mice at 5 months p.i. (3 independent experiments, n=16–20 mice per group).
(G) Frequency of cortical granulomas and **(H)** serum corticosterone levels after ACTH stimulation test in *Aire*$^{+/+}$ and *Aire*$^{-/-}$ mice at 5 months p.i. *Aire*$^{+/-}$ mice without immunization served as non-treated control (NT) (2 independent experiments, n=6–16 mice per group).
(I) Frequency of cortical granulomas in *Tnfr1*$^{+/+}$, *Tnfr1*$^{+/-}$ and *Tnfr1*$^{-/-}$ mice at 5 months p.i. (5 independent experiments, n=13–23 mice per group).
In **(E-I)** statistical significance was determined using the two-tailed Mann–Whitney test; P values are indicated. Bars show the mean ± SEM; individual mice are shown as symbols.

Figure 5. CD4$^+$ T cell-derived IFNG drives pathology in adoptive EAA model.
(A) Experimental outline of the adoptive EAA model. CYP11A1-restimulated activated CD4$^+$ T cells were transferred into immunodeficient hosts (*Rag2*$^{-/-}$ or *Cd3e*$^{-/-}$) prior to EAA induction.
(B) Serum corticosterone levels following ACTH stimulation test in *Rag2*$^{-/-}$ (2 independent experiments, n=9–12 mice per group) and *Cd3e*$^{-/-}$ (2 independent experiments, n=7–8 mice per group) recipients at 3 months post-transfer.
(C) Frequency of cortical granulomas in adrenal glands of *Rag2*$^{-/-}$ (2 independent experiments, n=7–11 mice per group) and *Cd3e* $^{-/-}$ (2 independent experiments, n=7–8 mice per group) mice at 3 months post-transfer.
(D) Representative H&E staining of adrenal sections from *Rag2*$^{-/-}$ recipients at 3 months post-transfer (2 independent experiments, n=7–11 mice per group). Whole-organ view (scale bar: 200µm) and magnified view (scale bar: 100µm) are shown. Adrenal borders, medulla, and granulomas are highlighted in yellow. Asterisks indicate infiltrating leukocytes.
(E) Quantification of CD45$^+$ and frequency of CD4$^+$ T-cell infiltration in adrenal glands of *Rag2*$^{-/-}$ recipients at 3 months post-transfer (2 independent experiments; n=10–11 mice per group).
(F) Serum corticosterone levels following ACTH stimulation test and **(G)** frequency of cortical granulomas following adoptive transfer of CD4$^+$ T cells from *Ifng*$^{+/+}$ or *Ifng*$^{-/-}$ donors into *Rag2*$^{-/-}$ recipients 3 months post-transfer (2 independent experiments; n=9–12 mice per group). NT represents *Rag2*$^{-/-}$ mice without adoptive transfer.
(H) Quantification of CD4$^+$ T cells and **(I)** effector CD4$^+$ T-cell subsets infiltrating adrenal glands of *Rag2*$^{-/-}$ recipients as in **(F)**. NT group was not analyzed due to the absence of endogenous T cells.
In (**B-C**, **E-I**) statistical significance was determined using the two-tailed Mann–Whitney test; P values are indicated. Bars show the mean ± SEM; individual mice are shown as symbols.

References

Ahonen, P., Myllarniemi, S., Sipila, I., and Perheentupa, J. (1990). Clinical variation of autoimmune polyendocrinopathy-candidiasis-ectodermal dystrophy (APECED) in a series of 68 patients. N Engl J Med *322*, 1829-1836.

Anderson, M.S., Venanzi, E.S., Klein, L., Chen, Z., Berzins, S.P., Turley, S.J., von Boehmer, H., Bronson, R., Dierich, A., Benoist, C., and Mathis, D. (2002). Projection of an immunological self shadow within the thymus by the aire protein. Science *298*, 1395-1401.

Betterle, C., Dal Pra, C., Mantero, F., and Zanchetta, R. (2002). Autoimmune adrenal insufficiency and autoimmune polyendocrine syndromes: autoantibodies, autoantigens, and their applicability in diagnosis and disease prediction. Endocr Rev *23*, 327-364.

Betterle, C., Zanette, F., Zanchetta, R., Pedini, B., Trevisan, A., Mantero, F., and Rigon, F. (1983). Complement-fixing adrenal autoantibodies as a marker for predicting onset of idiopathic Addison's disease. Lancet *1*, 1238-1241.

Bolotin, D.A., Poslavsky, S., Mitrophanov, I., Shugay, M., Mamedov, I.Z., Putintseva, E.V., and Chudakov, D.M. (2015). MiXCR: software for comprehensive adaptive immunity profiling. Nat Methods *12*, 380-381.

Bornstein, S.R., Allolio, B., Arlt, W., Barthel, A., Don-Wauchope, A., Hammer, G.D., Husebye, E.S., Merke, D.P., Murad, M.H., Stratakis, C.A., and Torpy, D.J. (2016). Diagnosis and Treatment of Primary Adrenal Insufficiency: An Endocrine Society Clinical Practice Guideline. J Clin Endocrinol Metab *101*, 364-389.

Bornstein, S.R., Malyukov, M., Heller, C., Ziegler, C.G., Ruiz-Babot, G., Schedl, A., Ludwig, B., and Steenblock, C. (2020). New Horizons: Novel Adrenal Regenerative Therapies. J Clin Endocrinol Metab *105*.

Borst, K., Flindt, S., Blank, P., Larsen, P.K., Chhatbar, C., Skerra, J., Spanier, J., Hirche, C., Konig, M., Alanentalo, T.*, et al.* (2020). Selective reconstitution of IFNgamma gene function in Ncr1+ NK cells is sufficient to control systemic vaccinia virus infection. PLoS Pathog *16*, e1008279.

Bradley, J.R. (2008). TNF-mediated inflammatory disease. J Pathol *214*, 149-160.

Bratland, E., and Husebye, E.S. (2011). Cellular immunity and immunopathology in autoimmune Addison's disease. Mol Cell Endocrinol *336*, 180-190.

Bratland, E., Skinningsrud, B., Undlien, D.E., Mozes, E., and Husebye, E.S. (2009). T cell responses to steroid cytochrome P450 21-hydroxylase in patients with autoimmune primary adrenal insufficiency. J Clin Endocrinol Metab *94*, 5117-5124.

Brennecke, P., Reyes, A., Pinto, S., Rattay, K., Nguyen, M., Kuchler, R., Huber, W., Kyewski, B., and Steinmetz, L.M. (2015). Single-cell transcriptome analysis reveals coordinated ectopic gene-expression patterns in medullary thymic epithelial cells. Nat Immunol *16*, 933-941.

Brozzetti, A., Marzotti, S., La Torre, D., Bacosi, M.L., Morelli, S., Bini, V., Ambrosi, B., Giordano, R., Perniola, R., De Bellis, A.*, et al.* (2010). Autoantibody responses in autoimmune ovarian insufficiency and in Addison's disease are IgG1 dominated and suggest a predominant, but not exclusive, Th1 type of response. Eur J Endocrinol *163*, 309-317.

Chen, S., Sawicka, J., Betterle, C., Powell, M., Prentice, L., Volpato, M., Rees Smith, B., and Furmaniak, J. (1996). Autoantibodies to steroidogenic enzymes in autoimmune polyglandular syndrome, Addison's disease, and premature ovarian failure. J Clin Endocrinol Metab *81*, 1871-1876.

Coco, G., Dal Pra, C., Presotto, F., Albergoni, M.P., Canova, C., Pedini, B., Zanchetta, R., Chen, S., Furmaniak, J., Rees Smith, B.*, et al.* (2006). Estimated risk for developing autoimmune Addison's disease in patients with adrenal cortex autoantibodies. J Clin Endocrinol Metab *91*, 1637-1645.

Dawoodji, A., Chen, J.L., Shepherd, D., Dalin, F., Tarlton, A., Alimohammadi, M., Penna-Martinez, M., Meyer, G., Mitchell, A.L., Gan, E.H.*, et al.* (2014). High frequency of cytolytic 21-hydroxylase-specific CD8+ T cells in autoimmune Addison's disease patients. J Immunol *193*, 2118-2126.

Derbinski, J., Pinto, S., Rosch, S., Hexel, K., and Kyewski, B. (2008). Promiscuous gene expression patterns in single medullary thymic epithelial cells argue for a stochastic mechanism. Proc Natl Acad Sci U S A *105*, 657-662.

Dineen, R., Thompson, C.J., and Sherlock, M. (2019). Adrenal crisis: prevention and management in adult patients. Ther Adv Endocrinol Metab *10*, 2042018819848218.

Dolfi, B., Gallerand, A., Firulyova, M.M., Xu, Y., Merlin, J., Dumont, A., Castiglione, A., Vaillant, N., Quemener, S., Gerke, H.*, et al.* (2022). Unravelling the sex-specific diversity and functions of adrenal gland macrophages. Cell Rep *39*, 110949.

Drobek, A., Moudra, A., Mueller, D., Huranova, M., Horkova, V., Pribikova, M., Ivanek, R., Oberle, S., Zehn, D., McCoy, K.D.*, et al.* (2018). Strong homeostatic TCR signals induce formation of self-tolerant virtual memory CD8 T cells. Embo J *37*.

Erichsen, M.M., Lovas, K., Skinningsrud, B., Wolff, A.B., Undlien, D.E., Svartberg, J., Fougner, K.J., Berg, T.J., Bollerslev, J., Mella, B.*, et al.* (2009). Clinical, immunological, and genetic features of autoimmune primary adrenal insufficiency: observations from a Norwegian registry. J Clin Endocrinol Metab *94*, 4882-4890.

Ferre, E.M., Rose, S.R., Rosenzweig, S.D., Burbelo, P.D., Romito, K.R., Niemela, J.E., Rosen, L.B., Break, T.J., Gu, W., Hunsberger, S.*, et al.* (2016). Redefined clinical features and diagnostic criteria in autoimmune polyendocrinopathy-candidiasis-ectodermal dystrophy. JCI Insight *1*.

Finnish-German, A.C. (1997). An autoimmune disease, APECED, caused by mutations in a novel gene featuring two PHD-type zinc-finger domains. Nat Genet *17*, 399-403.

Freedman, B.D., Kempna, P.B., Carlone, D.L., Shah, M., Guagliardo, N.A., Barrett, P.Q., Gomez-Sanchez, C.E., Majzoub, J.A., and Breault, D.T. (2013). Adrenocortical zonation results from lineage conversion of differentiated zona glomerulosa cells. Dev Cell *26*, 666-673.

Fujii, Y., Kato, N., Kito, J., Asai, J., and Yokochi, T. (1992). Experimental autoimmune adrenalitis: a murine model for Addison's disease. Autoimmunity *12*, 47-52.

Grabek, A., Dolfi, B., Klein, B., Jian-Motamedi, F., Chaboissier, M.C., and Schedl, A. (2019). The Adult Adrenal Cortex Undergoes Rapid Tissue Renewal in a Sex-Specific Manner. Cell Stem Cell *25*, 290-296 e292.

Grouthier, V., Lebrun-Vignes, B., Moey, M., Johnson, D.B., Moslehi, J.J., Salem, J.E., and Bachelot, A. (2020). Immune Checkpoint Inhibitor-Associated Primary Adrenal Insufficiency: WHO VigiBase Report Analysis. Oncologist *25*, 696-701.

Hao, Y., Hao, S., Andersen-Nissen, E., Mauck, W.M., 3rd, Zheng, S., Butler, A., Lee, M.J., Wilk, A.J., Darby, C., Zager, M.*, et al.* (2021). Integrated analysis of multimodal single-cell data. Cell *184*, 3573-3587 e3529.

Hao, Z., and Rajewsky, K. (2001). Homeostasis of peripheral B cells in the absence of B cell influx from the bone marrow. J Exp Med *194*, 1151-1164.

Hayashi, Y., Hiyoshi, T., Takemura, T., Kurashima, C., and Hirokawa, K. (1989). Focal lymphocytic infiltration in the adrenal cortex of the elderly: immunohistological analysis of infiltrating lymphocytes. Clin Exp Immunol *77*, 101-105.

Howe, K.L., Achuthan, P., Allen, J., Allen, J., Alvarez-Jarreta, J., Amode, M.R., Armean, I.M., Azov, A.G., Bennett, R., Bhai, J.*, et al.* (2021). Ensembl 2021. Nucleic Acids Res *49*, D884-D891.

Hubert, F.X., Kinkel, S.A., Crewther, P.E., Cannon, P.Z., Webster, K.E., Link, M., Uibo, R., O'Bryan, M.K., Meager, A., Forehan, S.P.*, et al.* (2009). Aire-deficient C57BL/6 mice mimicking the common human 13-base pair deletion mutation present with only a mild autoimmune phenotype. J Immunol *182*, 3902-3918.

Husebye, E.S., Pearce, S.H., Krone, N.P., and Kampe, O. (2021). Adrenal insufficiency. Lancet *397*, 613-629.

Husebye, E.S., Perheentupa, J., Rautemaa, R., and Kampe, O. (2009). Clinical manifestations and management of patients with autoimmune polyendocrine syndrome type I. J Intern Med *265*, 514-529.

Johannsson, G., Falorni, A., Skrtic, S., Lennernas, H., Quinkler, M., Monson, J.P., and Stewart, P.M. (2015). Adrenal insufficiency: review of clinical outcomes with current glucocorticoid replacement therapy. Clin Endocrinol (Oxf) *82*, 2-11.

Kanczkowski, W., Chatzigeorgiou, A., Samus, M., Tran, N., Zacharowski, K., Chavakis, T., and Bornstein, S.R. (2013). Characterization of the LPS-induced inflammation of the adrenal gland in mice. Mol Cell Endocrinol *371*, 228-235.

Kemp, W.L., Koponen, M.A., and Meyers, S.E. (2016). Addison Disease: The First Presentation of the Condition May be at Autopsy. Acad Forensic Pathol *6*, 249-257.

Kobza, A.O., Herman, D., Papaioannou, A., Lau, A.N., and Adachi, J.D. (2021). Understanding and Managing Corticosteroid-Induced Osteoporosis. Open Access Rheumatol *13*, 177-190.

Krywanczyk, A., and Bundock, E.A. (2017). Fatal Rotavirus Infection in a 4-Year-Old with Unsuspected Autoimmune Adrenal Insufficiency. Acad Forensic Pathol *7*, 130-135.

Kumai, T., Lee, S., Cho, H.I., Sultan, H., Kobayashi, H., Harabuchi, Y., and Celis, E. (2017). Optimization of Peptide Vaccines to Induce Robust Antitumor CD4 T-cell Responses. Cancer Immunol Res *5*, 72-83.

Laureti, S., De Bellis, A., Muccitelli, V.I., Calcinaro, F., Bizzarro, A., Rossi, R., Bellastella, A., Santeusanio, F., and Falorni, A. (1998). Levels of adrenocortical autoantibodies correlate with the degree of adrenal dysfunction in subjects with preclinical Addison's disease. J Clin Endocrinol Metab *83*, 3507-3511.

Lefranc, M.P., Giudicelli, V., Duroux, P., Jabado-Michaloud, J., Folch, G., Aouinti, S., Carillon, E., Duvergey, H., Houles, A., Paysan-Lafosse, T.*, et al.* (2015). IMGT(R), the international ImMunoGeneTics information system(R) 25 years on. Nucleic Acids Res *43*, D413-422.

Mateska, I., Witt, A., Hagag, E., Sinha, A., Yilmaz, C., Thanou, E., Sun, N., Kolliniati, O., Patschin, M., Abdelmegeed, H.*, et al.* (2023). Succinate mediates inflammation-induced adrenocortical dysfunction. Elife *12*.

Mitchell, A.L., and Pearce, S.H. (2012). Autoimmune Addison disease: pathophysiology and genetic complexity. Nat Rev Endocrinol *8*, 306-316.

Nagamine, K., Peterson, P., Scott, H.S., Kudoh, J., Minoshima, S., Heino, M., Krohn, K.J., Lalioti, M.D., Mullis, P.E., Antonarakis, S.E.*, et al.* (1997). Positional cloning of the APECED gene. Nat Genet *17*, 393-398.

Napier, C., Gan, E.H., Mitchell, A.L., Gilligan, L.C., Rees, D.A., Moran, C., Chatterjee, K., Vaidya, B., James, R.A., Mamoojee, Y., *et al.* (2020). Residual Adrenal Function in Autoimmune Addison's Disease-Effect of Dual Therapy With Rituximab and Depot Tetracosactide. J Clin Endocrinol Metab *105*.

Nishijima, H., Matsumoto, M., Morimoto, J., Hosomichi, K., Akiyama, N., Akiyama, T., Oya, T., Tsuneyama, K., Yoshida, H., and Matsumoto, M. (2022). Aire Controls Heterogeneity of Medullary Thymic Epithelial Cells for the Expression of Self-Antigens. J Immunol *208*, 303-320.

O'Brien, C.J., Sidarta-Oliveira, D., Stawiarski, A., Ratti, G., Loyher, P.-L., Makhlouf, M., AbouMoussa, E.H., Haberman, E., Sweeney, C., Mizuno, Y., *et al.* (2023). Distinct adrenal gland macrophages regulate corticosteroid production. bioRxiv, 2023.2009.2005.556330.

Oikonomou, V., Smith, G., Constantine, G.M., Schmitt, M.M., Ferre, E.M.N., Alejo, J.C., Riley, D., Kumar, D., Dos Santos Dias, L., Pechacek, J., *et al.* (2024). The Role of Interferon-gamma in Autoimmune Polyendocrine Syndrome Type 1. N Engl J Med *390*, 1873-1884.

Rottembourg, D., Deal, C., Lambert, M., Mallone, R., Carel, J.C., Lacroix, A., Caillat-Zucman, S., and le Deist, F. (2010). 21-Hydroxylase epitopes are targeted by CD8 T cells in autoimmune Addison's disease. J Autoimmun *35*, 309-315.

Ruedl, C., Khameneh, H.J., and Karjalainen, K. (2008). Manipulation of immune system via immortal bone marrow stem cells. Int Immunol *20*, 1211-1218.

Shen, F.W., Saga, Y., Litman, G., Freeman, G., Tung, J.S., Cantor, H., and Boyse, E.A. (1985). Cloning of Ly-5 cDNA. Proc Natl Acad Sci U S A *82*, 7360-7363.

Shih, M.C., Hsu, N.C., Huang, C.C., Wu, T.S., Lai, P.Y., and Chung, B.C. (2008). Mutation of mouse Cyp11a1 promoter caused tissue-specific reduction of gene expression and blunted stress response without affecting reproduction. Mol Endocrinol *22*, 915-923.

Sommers, C.L., Dejarnette, J.B., Huang, K., Lee, J., El-Khoury, D., Shores, E.W., and Love, P.E. (2000). Function of CD3 epsilon-mediated signals in T cell development. J Exp Med *192*, 913-919.

Tan, M.H., Iyengar, R., Mizokami-Stout, K., Yentz, S., MacEachern, M.P., Shen, L.Y., Redman, B., and Gianchandani, R. (2019). Spectrum of immune checkpoint inhibitors-induced endocrinopathies in cancer patients: a scoping review of case reports. Clin Diabetes Endocrinol *5*, 1.

Taves, M.D., Donahue, K.M., Bian, J., Cam, M.C., and Ashwell, J.D. (2023). Aire drives steroid hormone biosynthesis by medullary thymic epithelial cells. Sci Immunol *8*, eabo7975.

Tran, N.Q., Phan, C.C., Doan, T.T.P., and Tran, T.V. (2021). Bilateral adrenal masses due to tuberculosis: how to diagnose without extra-adrenal tuberculosis. Endocrinol Diabetes Metab Case Rep *2021*.

Ujevic, A., Knizkova, D., Synackova, A., Pribikova, M., Trivic, T., Dalinskaya, A., Drobek, A., Niederlova, V., Paprckova, D., De Guia, R., *et al.* (2024). TBK1-associated adapters TANK and AZI2 protect mice against TNF-induced cell death and severe autoinflammatory diseases. Nat Commun *15*, 10013.

Vinnard, C., and Blumberg, E.A. (2017). Endocrine and Metabolic Aspects of Tuberculosis. Microbiol Spectr *5*.

Vita, R., Mahajan, S., Overton, J.A., Dhanda, S.K., Martini, S., Cantrell, J.R., Wheeler, D.K., Sette, A., and Peters, B. (2019). The Immune Epitope Database (IEDB): 2018 update. Nucleic Acids Res *47*, D339-D343.

Winqvist, O., Karlsson, F.A., and Kampe, O. (1992). 21-Hydroxylase, a major autoantigen in idiopathic Addison's disease. Lancet *339*, 1559-1562.

Figure 1

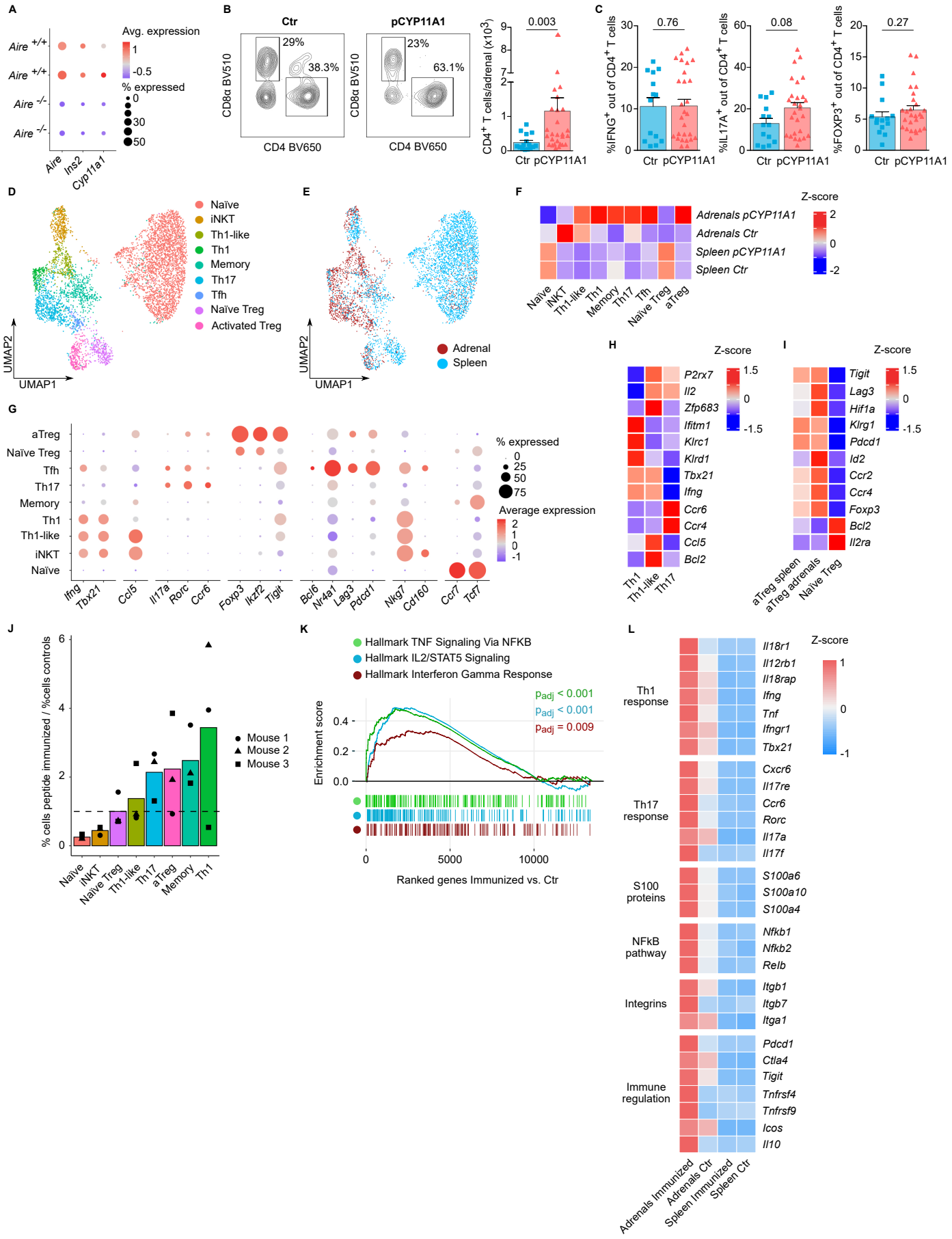
A
Avg. expression
% expressed
Aire +/+
Aire +/+
Aire -/-
Aire -/-
Aire
Ins2
Cyp11a1
B
Ctr
pCYP11A1
29%
38.3%
23%
63.1%
CD8α BV510
CD4 BV650
CD4+ T cells/adrenal (x10^3)
0.003
Ctr
pCYP11A1
C
%IFNG+ out of CD4+ T cells
0.76
%IL17A+ out of CD4+ T cells
0.08
%FOXP3+ out of CD4+ T cells
0.27
D
Naïve
iNKT
Th1-like
Th1
Memory
Th17
Tfh
Naïve Treg
Activated Treg
UMAP2
UMAP1
E
Adrenal
Spleen
F
Z-score
Adrenals pCYP11A1
Adrenals Ctr
Spleen pCYP11A1
Spleen Ctr
Naïve
iNKT
Th1-like
Th1
Memory
Th17
Tfh
Naïve Treg
aTreg
G
aTreg
Naïve Treg
Tfh
Th17
Memory
Th1
Th1-like
iNKT
Naïve
Ifng
Tbx21
Ccl5
Il17a
Rorc
Ccr6
Foxp3
Ikzf2
Tigit
Bcl6
Nr4a1
Lag3
Pdcd1
Nkg7
Cd160
Ccr7
Tcf7
% expressed
Average expression
H
Z-score
P2rx7
Il2
Zfp683
Ifitm1
Klrc1
Klrd1
Tbx21
Ifng
Ccr6
Ccr4
Ccl5
Bcl2
Th1
Th1-like
Th17
I
Z-score
Tigit
Lag3
Hif1a
Klrg1
Pdcd1
Id2
Ccr2
Ccr4
Foxp3
Bcl2
Il2ra
aTreg spleen
aTreg adrenals
Naïve Treg
J
% cells peptide immunized / %cells controls
Mouse 1
Mouse 2
Mouse 3
Naïve
iNKT
Naïve Treg
Th1-like
Th17
aTreg
Memory
Th1
K
Hallmark TNF Signaling Via NFKB
Hallmark IL2/STAT5 Signaling
Hallmark Interferon Gamma Response
padj < 0.001
padj < 0.001
padj = 0.009
Enrichment score
Ranked genes Immunized vs. Ctr
L
Z-score
Th1 response
Il18r1
Il12rb1
Il18rap
Ifng
Tnf
Ifngr1
Tbx21
Th17 response
Cxcr6
Il17re
Ccr6
Rorc
Il17a
Il17f
S100 proteins
S100a6
S100a10
S100a4
NFkB pathway
Nfkb1
Nfkb2
Relb
Integrins
Itgb1
Itgb7
Itga1
Immune regulation
Pdcd1
Ctla4
Tigit
Tnfrsf4
Tnfrsf9
Icos
Il10
Adrenals Immunized
Adrenals Ctr
Spleen Immunized
Spleen Ctr

Figure 2

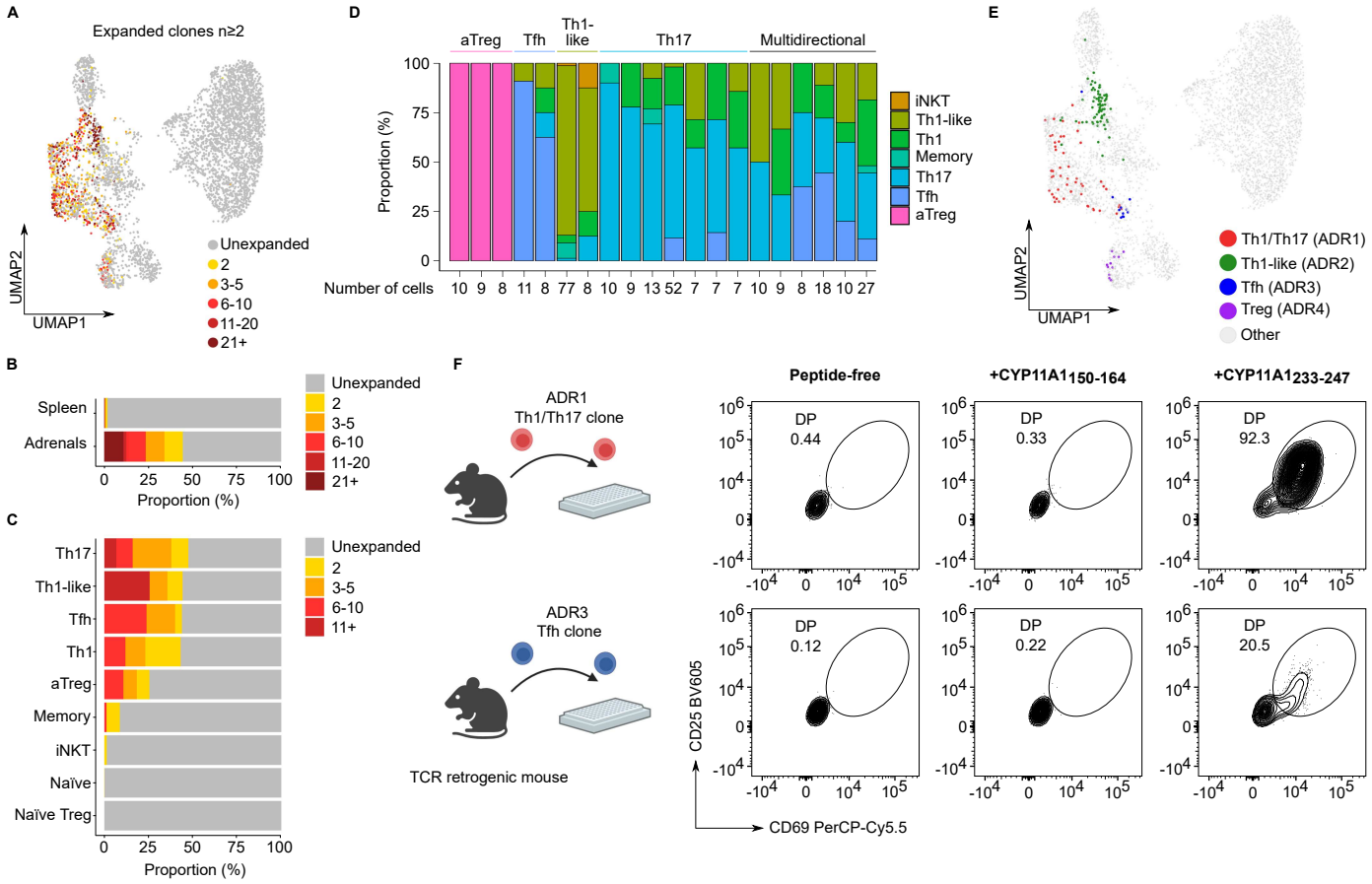
A
Expanded clones n≥2
UMAP2
UMAP1
Unexpanded
2
3-5
6-10
11-20
21+
D
aTreg
Tfh
Th1-like
Th17
Multidirectional
Proportion (%)
Number of cells
10 9 8 11 8 77 8 10 9 13 52 7 7 7 10 9 8 18 10 27
iNKT
Th1-like
Th1
Memory
Th17
Tfh
aTreg
E
UMAP2
UMAP1
Th1/Th17 (ADR1)
Th1-like (ADR2)
Tfh (ADR3)
Treg (ADR4)
Other
B
Spleen
Adrenals
Proportion (%)
Unexpanded
2
3-5
6-10
11-20
21+
C
Th17
Th1-like
Tfh
Th1
aTreg
Memory
iNKT
Naïve
Naïve Treg
Proportion (%)
Unexpanded
2
3-5
6-10
11+
F
ADR1
Th1/Th17 clone
ADR3
Tfh clone
TCR retrogenic mouse
Peptide-free
+CYP11A1150-164
+CYP11A1233-247
DP
0.44
DP
0.33
DP
92.3
DP
0.12
DP
0.22
DP
20.5
CD25 BV605
CD69 PerCP-Cy5.5

Figure 3

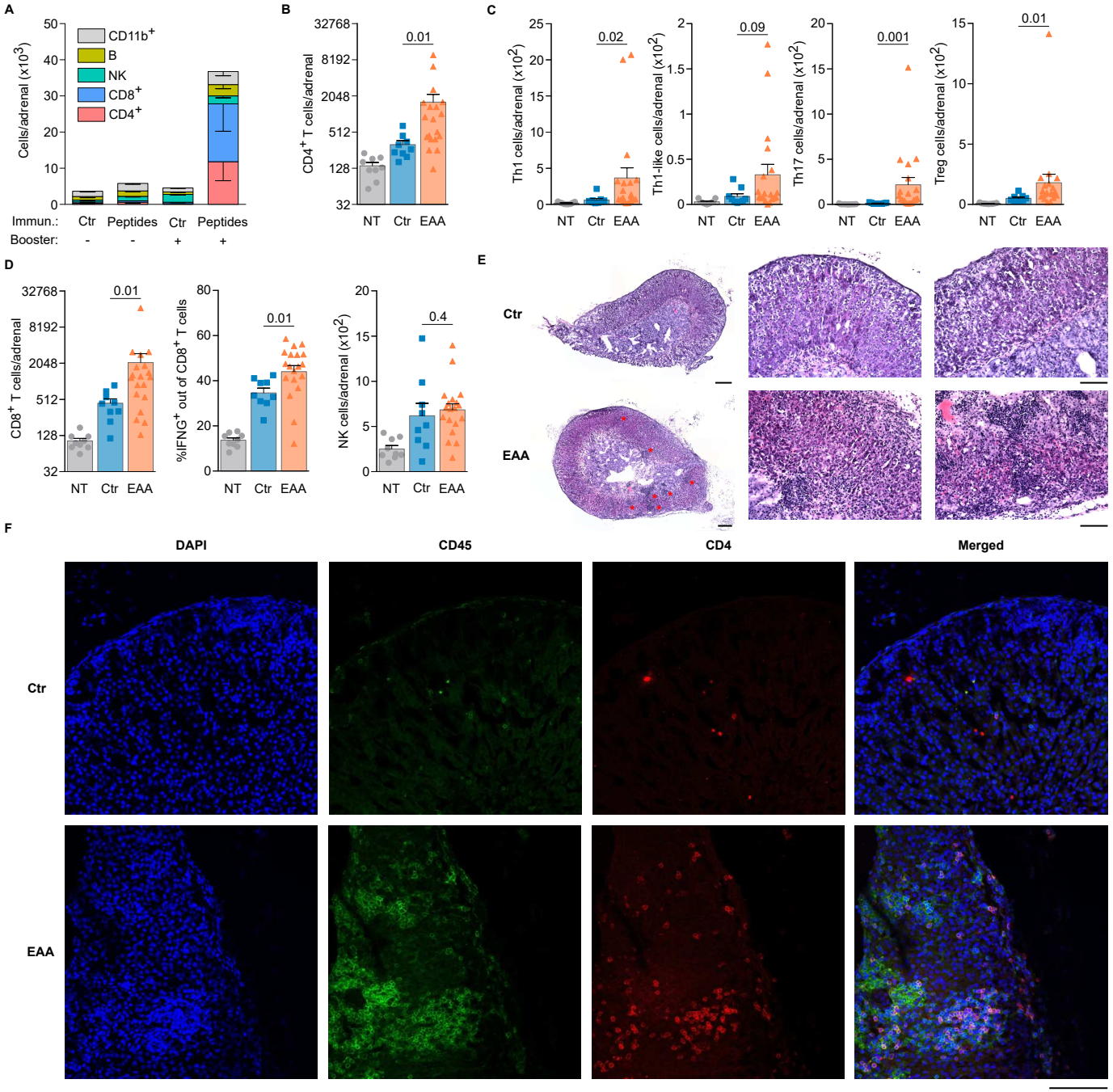
A
Cells/adrenal (x10^3)
CD11b+
B
NK
CD8+
CD4+
Immun.: Ctr Peptides Ctr Peptides
Booster: - - + +
B
CD4+ T cells/adrenal
0.01
NT Ctr EAA
C
Th1 cells/adrenal (x10^2)
0.02
Th1-like cells/adrenal (x10^2)
0.09
Th17 cells/adrenal (x10^2)
0.001
Treg cells/adrenal (x10^2)
0.01
NT Ctr EAA
D
CD8+ T cells/adrenal
0.01
%IFNG+ out of CD8+ T cells
0.01
NK cells/adrenal (x10^2)
0.4
NT Ctr EAA
E
Ctr
EAA
F
DAPI
CD45
CD4
Merged
Ctr
EAA

Figure 4

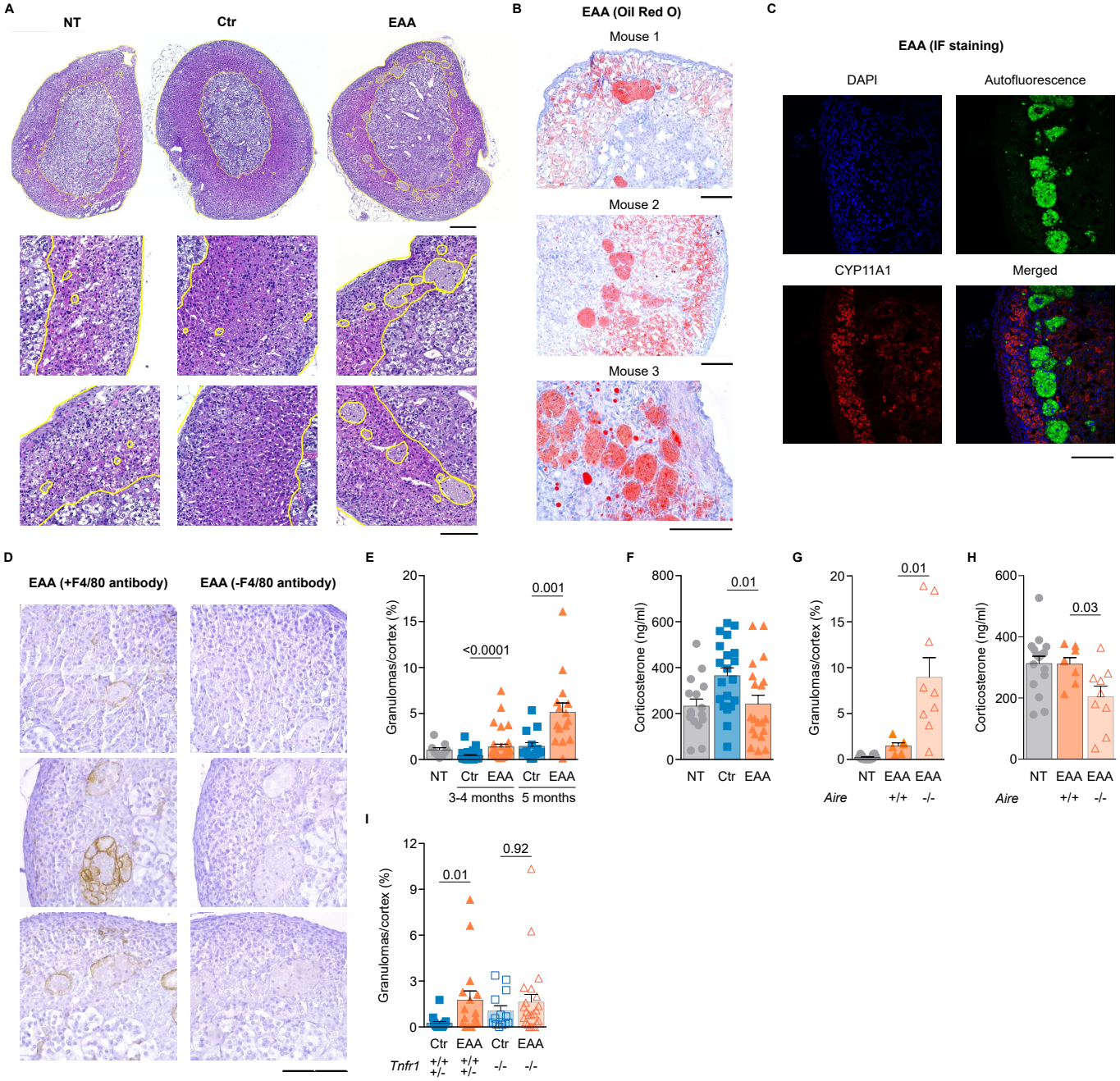
A
NT
Ctr
EAA
B
EAA (Oil Red O)
Mouse 1
Mouse 2
Mouse 3
C
EAA (IF staining)
DAPI
Autofluorescence
CYP11A1
Merged
D
EAA (+F4/80 antibody)
EAA (-F4/80 antibody)
E
Granulomas/cortex (%)
<0.0001
0.001
NT
Ctr
EAA
Ctr
EAA
3-4 months
5 months
F
Corticosterone (ng/ml)
0.01
NT
Ctr
EAA
G
Granulomas/cortex (%)
0.01
NT
EAA
EAA
Aire
+/+
-/-
H
Corticosterone (ng/ml)
0.03
NT
EAA
EAA
Aire
+/+
-/-
I
Granulomas/cortex (%)
0.01
0.92
Ctr
EAA
Ctr
EAA
Tnfr1
+/+ +/-
+/+ +/-
-/-
-/-

Figure 5

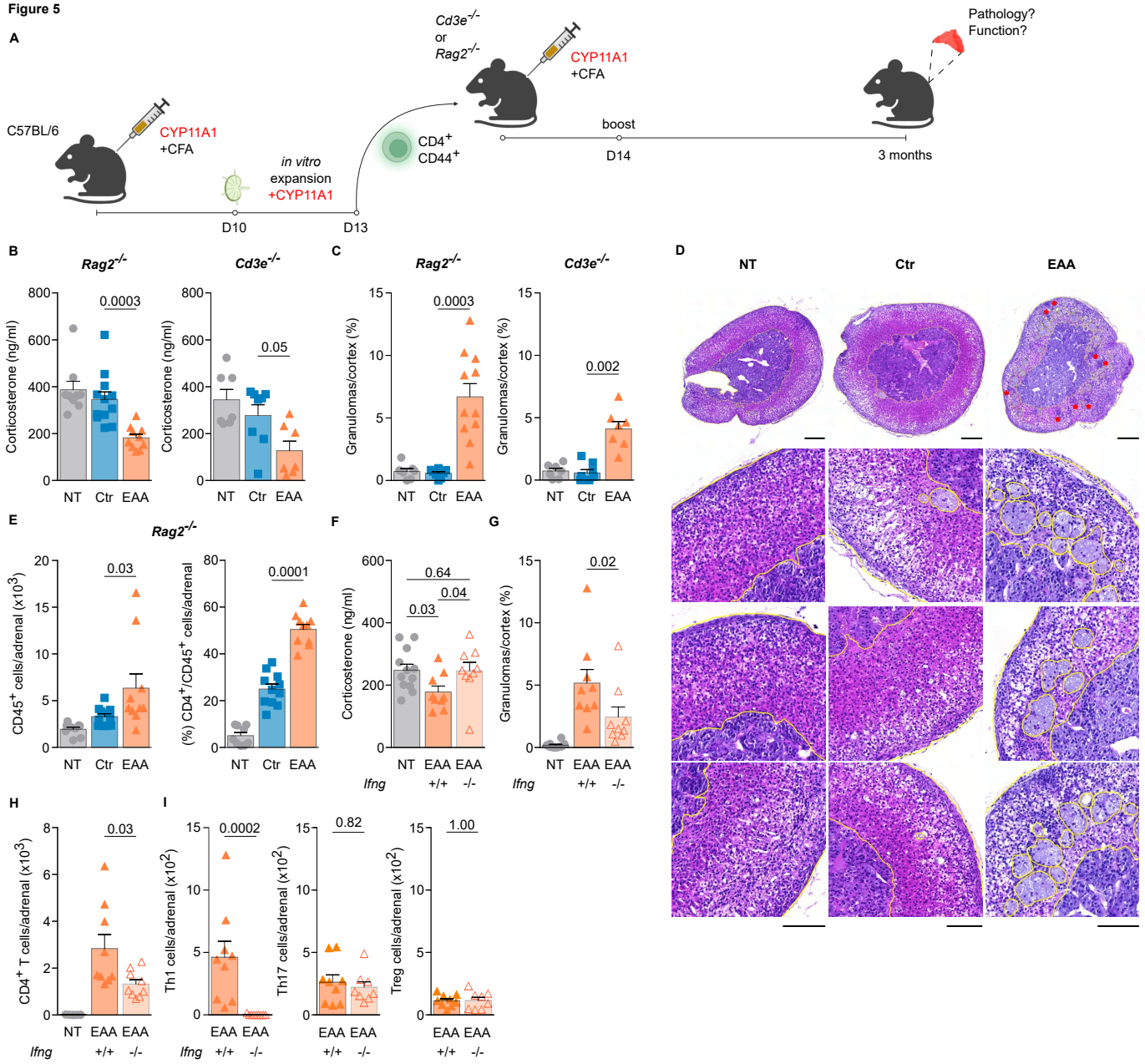
A
C57BL/6
CYP11A1
+CFA
in vitro
expansion
+CYP11A1
D10
D13
Cd3e-/-
or
Rag2-/-
CD4+
CD44+
CYP11A1
+CFA
boost
D14
3 months
Pathology?
Function?
B
Rag2-/-
Cd3e-/-
Corticosterone (ng/ml)
0.0003
0.05
NT Ctr EAA
C
Granulomas/cortex (%)
0.0003
0.002
D
NT
Ctr
EAA
E
CD45+ cells/adrenal (x10^3)
0.03
(%) CD4+/CD45+ cells/adrenal
0.0001
F
Corticosterone (ng/ml)
0.64
0.04
0.03
Ifng
+/+ -/-
G
Granulomas/cortex (%)
0.02
H
CD4+ T cells/adrenal (x10^3)
0.03
I
Th1 cells/adrenal (x10^2)
0.0002
Th17 cells/adrenal (x10^2)
0.82
Treg cells/adrenal (x10^2)
1.00